Journal of Inorganic Biochemistry 193 (2019) 70–83

Contents lists available at ScienceDirect

Journal of Inorganic Biochemistry

journal homepage: www.elsevier.com/locate/jinorgbio

Ru(II)/N-N/PPh_3 complexes as potential anticancer agents against MDA-MB-231 cancer cells (N-N = diimine or diamine)

Gabriel H. Ribeiro[a,*], Legna Colina-Vegas[a], Juan C.T. Clavijo[b], Javier Ellena[b], Marcia R. Cominetti[c], Alzir A. Batista[a,*]

[a] Universidade Federal de São Carlos, Departamento de Química, São Carlos, SP, Brazil
[b] Instituto de Física de São Carlos, Universidade de São Paulo, São Carlos, SP, Brazil
[c] Universidade Federal de São Carlos, Departamento de Gerontologia, São Carlos, SP, Brazil

A B S T R A C T

The rational design of anticancer agents that acts in specific biological targets is one of the most effective strategies for developing chemotherapeutic agents. Aiming at obtaining new ruthenium (II) compounds with good cytotoxicity against tumor cells, a series of new complexes of general formula [RuCl(PPh_3)(Hdpa)(N—N)]Cl [PPh_3 = triphenylphosphine, N-N = 2,2′-dipyridylamine (Hdpa) (**1**), 1,2-diaminoethane (en) (**2**), 2,2′-bipyridine (bipy) (**3**), 5,5′-dimethyl-2,2′-bipyridine (dmbipy) (**4**), 1,10-phenanthroline (phen) (**5**) and 4,7-diphenyl-1,10-phenanthroline (dphphen) (**6**)] were synthesized. The complexes were characterized by elemental analysis and spectroscopic techniques (IR, UV/Visible, and 1D and 2D NMR) and three of their X-ray structures were determined: [RuCl(PPh_3)$(Hdpa)_2$]Cl, [RuCl(PPh_3)(Hdpa)(en)]Cl and [RuCl(PPh_3)(Hdpa)(dmbipy)]Cl. All the complexes are more cytotoxic against the cancer cell line than against the non-tumor cell line, highlighting complexes **1** and **5,** which have an index selectivity of 18 and 15, respectively. The binding constants of compounds **1–6** with human serum albumin (HSA) were determined by tryptophan fluorescence quenching, indicating moderate to strong interactions. The binding mode of the complexes to calf thymus (CT) DNA was explored by several techniques, which reveal that only the dphphen compound **6** causes distortions in the secondary and tertiary structures of DNA. The studies demonstrated that the nature of the N—N co-ligand and the presence of the PPh_3 and Hdpa ligands are features that can influence the binding affinity of the complexes by the biomolecules and in the cytotoxic activity of the complexes. Overall, the complexes with diimine co-ligand are much more cytotoxic than compound **2** with the aliphatic diamine.

1. Introduction

Currently, ruthenium-based complexes represent promising alternative candidates to platinum drugs, with less toxic side effects and more selectivity against cancer cells than against non-tumor cells [1–6]. Moreover, ruthenium complexes can act by a myriad of biological targets, such as proteins, membranes, DNA, etc. [7–12]. In this context, the synthesis of new ruthenium polypyridyl compounds capable of targeting DNA has been widely investigated in recent years [13–17]. These kinds of complexes have been shown to bind to DNA by various modes [10,13], e.g., through intercalation of the polypyridyl ligand in the base pairs of DNA [18,19] or via association with the minor or major grooves [20]. Binding compounds to DNA grooves can exhibit high levels of DNA sequence-specific recognition [13] due to many base pairs found in the biomolecule, and also by the possible combination of Van der Waals interactions, hydrogen bonding, hydrophobic contacts and electrostatic interactions [13,20,21]. Ruthenium complexes such as $[Ru(bipy)_3]^{2+}$ and $[Ru(Me_4phen)_3]^{2+}$ (bipy = 2,2′-bipyridine; Me_4phen = 3,4,7,8-tetramethyl-phenanthroline) associate electrostatically within the grooves of the DNA, without disrupting its double helix, despite the presence of ligands that usually intercalate DNA [10].

In recent years, our research group has been attracted by the possibilities of multifunctional chemotherapy. In this context, we have synthesized new ruthenium(II)/phosphine complexes containing diimine ligands and various other classes of ligands, aiming at identifying synergisms between the metallic center and functional ligands [22–25]. Thus, many compounds were synthesized, and some of them showed high cytotoxicity [25]. Recently, we reported on the compounds [Ru(pyS)(bipy)(dppb)]PF_6, [Ru(Spym)(bipy)(dppb)]PF_6 and [Ru(SpymMe$_2$)(bipy)(dppb)]PF_6 [dppb = 1,4-Bis(diphenylphosphino)butane; (pyS) = 2-mercaptopyridine; (Spym) = 2-mercaptopyrimidine and (SpymMe2) = 4,6-dimethyl-2-mercaptopyrimidine], which showed, in vitro, higher cytotoxicity against the HepG2 cell line than the cisplatin [24]. Furthermore, these compounds showed the property of inhibiting the DNA supercoiled relaxation mediated by the human topoisomerase IB and additional assays indicate that they inhibit the cleavage reaction, impeding the binding of the enzyme to DNA and slowing down the relegation reaction. Thus, results suggest that the topoisomerase I is one possible target for the synthesized complexes [24].

* Corresponding authors.
E-mail addresses: gabrielhenri10@hotmail.com (G.H. Ribeiro), daab@ufscar.br (A.A. Batista).

https://doi.org/10.1016/j.jinorgbio.2019.01.006
Received 9 August 2018; Received in revised form 10 January 2019; Accepted 12 January 2019
Available online 18 January 2019
0162-0134/

In this study, based on the knowledge gained by our research group with ruthenium (II) complexes, a series of [RuCl(PPh_3)(Hdpa)(N—N)]Cl complexes [PPh_3 = triphenylphosphine; N-N = 2,2′-dipyridylamine (Hdpa), 1,2-diaminoethane (en), 2,2′-bipyridine (bipy), 5,5′-dimethyl-2,2′-bipyridine (dmbipy), 1,10-phenanthroline (phen) and 4,7-diphenyl-1,10-phenanthroline (dphphen)] were synthesized and characterized. The inspiration for the design of these complexes was: (a) the fact that using hydrophobic PPh_3 ligand results in complexes with good cytotoxicity, presumably because of increasing vehiculation property of the complexes [23,26]; (b) the ligand Hdpa can provide a good solubility to the complexes in polar solvents, due to the presence of the NH group in its structure [14,27–29]; (c) we focused mainly on assessing whether design modification of the N—N co-ligands (comparison between the diimine ligands and aliphatic bidentate diamine ligand and with different numbers of aromatic rings) can lead to modulating the binding mode to biomolecules and biological activity of the compounds; (d) using chloride as a labile ligand and as a hydrogen-bond acceptor might be able to form additional hydrogen bonds, such as O—H···Cl, N—H···Cl, and C—H···Cl, with biomolecules facilitating the interaction of complex/DNA [30].

Herein the binding mode of the new complexes with DNA was also investigated by using a variety of methods, such as absorption spectroscopy (UV/Vis and circular dichroism), viscosity measurements and gel electrophoresis of DNA plasmid. Interaction of the compounds with other relevant biomolecules, human serum albumin (HSA) by fluorescence quenching, was also evaluated with the aim of initially understanding the pharmacological properties of the compounds. The cytotoxicity of the compounds in vitro was examined by MTT (3-(4,5-dimethylthiazol-2-yl)-2,5-diphenyltetrazolium bromide) assay, against the tumor cell line (MDA-MB-231) and the non-tumor cell line (V79–4).

2. Experimental section

$RuCl_3.3H_2O$, 2,2′-dipyridylamine, 1,10-phenanthroline, 2,2′-bipyridine, 4,7-diphenyl-1,10-phenanthroline, 4,4′-dimethyl-2,2′-bipyridine, 1,2-diaminoethane and triphenylphosphine were obtained from Sigma-Aldrich. All chemicals were used as purchased, without further purification.

Monodimensional [^{1}H, ^{13}C{^{1}H}, ^{31}P{^{1}H}] and bidimensional [^{1}H—^{1}H correlation spectroscopy (COSY), ^{1}H - ^{13}C {^{1}H} heteronuclear single-quantum correlation (HSQC), ^{1}H - ^{13}C {^{1}H} heteronuclear multiple-bond correlation (HMBC)] nuclear magnetic resonance (NMR) experiments were recorded on a Bruker DRX-400 spectrometer (9.4 T) equipped with an inverse 5 mm probe head with an actively shielded z-gradient coil. ^{1}H and ^{13}C {^{1}H} chemical shifts in dimethyl sulfoxide (DMSO-d_6) were referenced to the peak of a residual non-deuterated solvent [(^{1}H) δ 2.50, and (^{13}C{^{1}H}) δ 39.52 for DMSO-d_6]. The ^{31}P{^{1}H} NMR spectra were carried out in dimethyl sulfoxide (DMSO-d_6) (using a capillary containing H_3PO_4 85% in D_2O) and the chemical shifts were referenced to an external 85% H_3PO_4 standard at 0.00 ppm.

Elemental analyses were performed on a FISIONS Instrument EA 1108 CHNS elemental analyzer at the Microanalytical Laboratory at the Federal University of São Carlos, São Carlos (SP). Conductivity measurements in water and dimethyl sulfoxide solutions (1.0 mmol L^{-1}) of the complexes were carried out on a Meter Lab CDM2300 conductivity meter using a cell of constant 0.089 cm^{-1}. FTIR spectra were recorded on a Bomem-Michelson 102 spectrometer in the range of 4000–200 cm^{-1}. The samples were examined in CsI cells. UV–visible absorption spectra were recorded using a Varian model Cary 500 NIR spectrophotometer with 1.0 cm quartz cell in the range of 240–800 nm. Electrochemical measurements were carried out using a 100 B/W electrochemical workstation from Bioanalytical Systems with a conventional three-electrode system. Scans were recorded on samples dissolved in dichloromethane containing 0.1 mol L^{-1} tetrabutylammonium perchlorate (PTBA Fluka Purum) solution. The working and auxiliary electrodes were of platinum and Ag/AgCl, 0.10 mol L^{-1} PTBA in dichloromethane as the reference electrode. Under these conditions, the ferrocene/ferrocenium oxidation occurs at 0.43 V.

2.1. Single crystal X-ray structure data analysis

Crystals of complex **1** were grown by slow evaporation of dichloromethane/methanol solution. The crystals of complexes **2** and **4** were grown in a solution of dichloromethane/methanol, but in these cases KPF_6 (1:1, complex/KPF_6) was added to the solution in order to facilitate the crystallization. The single crystals exhibited a prism form and were mounted on an Enraf-Nonius Kappa-CCD diffractometer with graphite monochromated Mo Kα radiation (λ = 0.71073 Å). The dimensions and the symmetry of the unit cell were measured based on all reflections. Data collection was performed at room temperature (293 K) after the unit cell dimensions were determined using the COLLECT program [31,32]. Integration and scaling of the reflections were carried out using the HKL Denzo-Scalepack software package [33]. The structures were solved through direct methods of phase retrieval with SHELXS-2013 [34] and the refinement by the full-matrix least-squares on F2 with SHELXL-20135 [34] within the WinGX-v.2013.3 [35] program package. Absorption correction was performed by the Gaussian method [35]. Non-hydrogen atoms were refined anisotropically and hydrogen atoms were fixed at calculated positions and refined using the riding mode. The constrained positions and fixed isotropic thermal parameters for C—H hydrogen atoms were the bond lengths of 0.93 and 0.97 Å for Csp^2 —H (aromatic rings) and Csp^3 —H (methylene groups), respectively, considering Uiso(H) = 1.2Ueq(C). Structure analysis and the preparation of artwork were performed using MERCURY and ORTEP-3 software [36]. WinGX was used to prepare the material for publication (CIF file). The crystallographic data are given in Table 1.

2.2. Synthesis

All synthetic procedures were carried out under argon atmosphere using standard Schlenk techniques. The precursors [$RuCl_2(PPh_3)_3$)], *cis*-[$RuCl_2(PPh_3)_2$(bipy)], *cis*-[$RuCl_2(PPh_3)_2$(dmbipy)], *cis*-[$RuCl_2(PPh_3)_2$(phen)], *cis*-[$RuCl_2(PPh_3)_2$(dphphen)] and *trans*-[$RuCl_2(PPh_3)_2$(en)] were synthesized as described in the literature [37–39].

2.2.1. [RuCl(PPh_3)(Hdpa)$_2$]Cl (1)

The Hdpa ligand (54 mg; 0.313 mmol) was added to a solution of [$RuCl_2(PPh_3)_3$] (150 mg; 0.156 mmol) in dichloromethane (15 mL). The resulting solution was stirred for 24 h at room temperature and an orange solid was precipitated. The solid was filtered off, washed with diethyl ether and dried in vacuo. Yield 94 mg (77%). Elemental analysis (%) Calc. for $C_{38}H_{33}Cl_2N_6PRu.^1/_3CH_2Cl_2$: C 57.20; H 4.19; N 10.21 Found: C 57.19; H 3.91; N 10.44. NMR-^{31}P {^{1}H} (DMSO-d_6) [δ/ppm (multiplicity, assignment)] 44.1 (s, PPh_3). NMR-^{1}H (DMSO-d_6) {[δ/ppm (multiplicity, integration, assignment, *J*/Hz, coordination-induced shifts (c.i.s), $\delta_{complex}$ - δ_{ligand}]} 11.09 (s, 1H, NH, 1.46), 10.51 (s, 1H, NH, 0.85), 8.70 (d, 1H, H6′, ^3J = 5.5, 0.49), 7.82 (d; 1H; H10′; ^3J = 4.8, 0.39), 7.68 (p, 2H, H8″/H12′), 7.61–7. 54 (m, 2H, H10″ e H12″), 7.38 (t, 1H, H8′, ^3J = 7.3, −0.25), 7.32–7.19 (m, 5H, H9″/H13′/H3), 7.18–7.11 (m, 2H, H6″/H13′), 7.09–6.94 (m, 12H, H2/H1), 6.73 (d, 1H, H9′, ^3J = 8.1, −1.01), 6.64 (t, 1H, H7″, ^3J = 6.3, −0.21), 6.56 (t, 1H, H7′,^3J = 6.4, −0.26), 6.49 (t, 1H, H11″, ^3J = 6.3; −0.36), 6.38 (t, 1H, H11′, ^3J = 6.3, −0.47). NMR-^{13}C {^{1}H} (DMSO-d_6) [δ/ppm (multiplicity, assignment)] 157.95 (s, C6′), 148.60 (s, C6″), 117.75 (s, C7′), 118.57 (s, C7″), 138.46 (s, C8′), 138.87 (s, C8″), 126.47 (s, C9′), 7.17 (s, C9″), 154.50 (dd, C10′/C10″), 115.51 (s, C11′), 113.50 (s, C11″), 136.42 (d, C12′/C12″), 123.86 (d, C13′/C13″), 133.58 (d, C1), 128.70 (d, C2), 130.34 (s, C3). Selected IR (CsI, cm^{-1}): *ν* (N—H) 3438 cm^{-1} *ν* (C═N) 1632 cm^{-1} *ν* (C═C) 1469 cm^{-1} ν_{as} (P—CH) 1087 cm^{-1} *ν* (Ru—N) 528 cm^{-1} *ν* (Ru—P) 511 cm^{-1}, *ν* (Ru—Cl) 230 cm^{-1}. UV/visible spectrum [CH_2Cl_2; λ_{max}, nm (ε, M^{-1} cm^{-1})]:

Table 1
Crystal data and structure refinement parameters obtained for complexes **1**, **2** and **4**.

Complex	(1)	(2)	(4)
Empirical formula	$C_{39}H_{35}Cl_4N_6PRuO$	$C_{31}H_{34}Cl_3N_5P_2RuF_6$	$C_{40}H_{36}ClN_5P_2RuO_2$
Formula weight (g/mol)	861.57	859.99	931.20
Crystal system	Monoclínic	Triclinic	Triclinic
Space group	P 21/c	P -1	P -1
a (Å)	11.11400(10)	10.1746(2)	10.661(2)
b (Å)	20.8490(2)	10.4747(2)	11.3252(2)
c (Å)	16.4720(3)	18.2349(4)	20.6240(5)
A	90°	104.7940(10)°	74.4130(10)°
B	90.5830 (10)°	105.4150(10)°	85.6900(10)°
Γ	90 (10)°	91.8940(10)°	64.132(2)°
Volume (Å^3)	3816.63(9)	1800.73(12)	2155.74(8)
Z	4	2	2
Density calculated (Mg/m^3)	1.499	1.586	1.435
Absorption coefficient (mm^{-1})	0.770	0.808	0.565
F (000)	1752	868	944
Crystal size (mm^3)	0.31 × 0.27 × 0.05	0.03 × 0.3 × 0.19	0.46 × 0.44 × 0.15
Θ range	5.918 to 52.73°	5.968 to 51.55°	6.052 to 51.362°
Index ranges	−13 ≤ h ≤ 13, −26 ≤ k ≤ 23, −19 ≤ l ≤ 20	−12 ≤ h ≤ 12, −12 ≤ k ≤ 12, −21 ≤ l ≤ 22	−13 ≤ h ≤ 12, −13 ≤ k ≤ 13, −25 ≤ l ≤ 25
Reflections collected	76,409	13,041	38,649
Independent reflections (Rint)	7789 (0.0365)	6864 (0.0283)	8161 (0.0257)
Completeness to θ(%)	99.8%	99.8%	99.8%
Data/restraints/parameters	7789/0/460	6864/0/434	8161/0/519
Goodness-of-fit on F^2	1.116	1.000	1.001
Final R índices [I > 2σ(I)]	R1 = 0.0373, w*R*2 = 0.0955	R1 = 0.0484, w*R*2 = 0.1270	R1 = 0.0428, wR2 = 0.1250
R indices (all data)	R1 = 0.0493, wR2 = 0.1018	R1 = 0.0560, wR2 = 0.1316	R1 = 0.0496, wR2 = 0.1293
$\Delta\rho_{max.}$ and $\Delta\rho_{min.}$(e. Å^{-3})	1.06 and − 0.58	1.30 and − 1.22	0.84 and − 0.70

298 (55905), 368 (16261), 430 (7951).

2.2.2. [RuCl(PPh$_3$)(Hdpa)(en)]Cl (2)

The Hdpa ligand (34 mg; 0.198 mmol) was added to a solution of [RuCl$_2$(PPh$_3$)$_2$(en)] (150 mg; 0.198 mmol) in dichloromethane (20 mL). The resulting solution was stirred for 48 h at room temperature, the solvent was removed under reduced pressure to ca. 2 mL and acetone was added for the precipitation of a yellow solid, which was filtered off, rinsed with acetone (5 × 5 mL) and dried in vacuo. Yield 91 mg (69%). Elemental analysis (%) Calc. for $C_{30}H_{32}Cl_2N_5PRu.{}^1/_{10}CH_2Cl_2$: C 53.72; H 4.81; N 10.37 found: C 53.69; H 5.09; N 10.21. NMR-^{31}P {^{1}H} (DMSO-d_6) [δ/ppm (multiplicity, assignment)] 53.9 (s, PPh$_3$). NMR-^{1}H (DMSO-d_6) [δ/ppm (multiplicity, integration, assignment, *J*/Hz, c.i.s)] 10.15 (s, 1H, NH, 0.51), 8. 86 (d, 1H, H6′, ^3J = 6.2, 0.65), 7.68 (d, 1H, H6″, ^3J = 5.7, −0.53), 7.51 (t, 1H, H8′, ^3J = 7.8; −0.12), 7.33–7.15 (m, 16H, H1/H2/H3/H8″), 6.98 (d, 1H, H9′, ^3J = 8.3, −0.76), 6.68 (d, 1H, H9″, ^3J = 8.2, −1.06), 6.46 (t, 1H, H7′, ^3J = 6.6, −0.39), 6.30 (t, 1H, H7″, ^3J = 6.4, −0.54), 4.85 [m, 1H, H10′ (NH$_2$)], 4.66 [m, 1H, H10″ (NH$_2$)], 4.40 [(m, 1H, H13′ (NH$_2$)], 3.17 [m, 1H, H13″ (NH$_2$)], 3.03 [m, 1H, H11′ (CH$_2$)], 2.85 [m, 1H, H12′ (CH$_2$)], 2.70 [m, 1H, H11″ (CH$_2$)], 2.25 [m, 1H, H12″ (CH$_2$)]. NMR-^{13}C {^{1}H} (DMSO-d_6) [δ/ppm (multiplicity, assignment)] 155.65 (s, C6′), 154.46 (s, C6″), 116.18 (s, C7′), 116.92 (s, C7″), 136.88 (s, C8′), 135.69 (s, C8″), 112.20 (s, C9′), 113.82 (s, C9″), 42.43 (s, C11′/C11″), 45.75 (s, C12′/C12″), 133.49 (d, C1), 128.00 (d, C2), 129.00 (s, C3). Selected IR (CsI, cm^{-1}): *ν* (N—H) 3437 cm^{-1} *ν* (C═N) 1641 cm^{-1} *ν* (C═C) 1481 cm^{-1} ν_{as} (P—CH) 1088 cm^{-1} *ν* (Ru—N) 529 cm^{-1} *ν* (Ru—P) 503 cm^{-1}, *ν* (Ru—Cl) 243 cm^{-1}. UV/visible spectrum [CH_2Cl_2; λ $_{max}$, nm (ε, M^{-1} cm^{-1})]: 301 (52980), 353 (9788).

2.2.3. [RuCl(PPh$_3$)(Hdpa)(bipy)]Cl (3)

The Hdpa ligand (45 mg; 0.264 mmol) was added to a yellow suspension of *cis*-[RuCl$_2$(PPh$_3$)$_2$(bipy)] (150 mg; 0.176 mmol) in dichloromethane/methanol (1/1, 30 mL). The mixture was refluxed for ca. 48 h under vigorous stirring, the solvent was removed under a reduced pressure to ca. 2 mL volume and diethyl ether was added for the precipitation of a red solid, which was filtered off, rinsed with diethyl ether (5 × 5 mL) to remove the excess of ligand and dried in vacuo. Yield 106 mg (79%). Elemental analysis (%) Calc. for $C_{38}H_{32}Cl_2N_5PRu.{}^1/_5CH_2Cl_2$: C 58.68; H 4.16; N 8.95 Found: C 58.77; H 4.16; N 8.81. NMR-^{31}P {^{1}H} (DMSO-d_6) [δ/ppm (multiplicity, assignment)] 41.5 (s, PPh$_3$). NMR-^{1}H (DMSO-d_6) [δ/ppm (multiplicity, integration, assignment, *J*/Hz, c.i.s)] 11.05 (s, 1H, NH, 1.42), 9.45 (d, 1H, H10′, ^3J = 5.5, 0.86), 8.55 (d, 1H, H10″, ^3J = 5.5, −0.03), 8.28 (d, 1H, H13′, ^3J = 8.0, −0.22), 8.19 (m, 2H, H13″/6″), 7.91 (t, 1H, H12′, ^3J = 7.7, 0.26), 7.80 (m, 2H, H8″/H12″), 7.59–7.51 (m, 2H, H8′/9″), 7.43 (t, 1H, H11′, ^3J = 6.5, 0.30), 7.32–7.27 (m, 6H, H1/H11″), 7.16 (m, 7H, H2, H6″/H9″), 6.97 (m, 5H, H3), 6.65 (t, 1H, H7″, ^3J = 6.5, −0.20), 6.6 (t, 1H, H7′, ^3J = 6.5, −0.27). NMR-^{13}C {^{1}H} (DMSO-d_6) [δ/ppm (multiplicity, assignment)] 157.95 (s, C6′), 148.60 (s, C6″), 117.75 (s, C7′), 118.57 (s, C7″), 138.46 (s, C8′), 138.87 (s, C8″), 115.51 (s. C9′), 113.50 (s, C9″), 154.50 (dd, C10′/C10″), 126.47 (s, C11′), 125.46 (s, C11″), 136.42 (d, C12′/C12″), 123.86 (d, C13′/C13″), 133.58 (d, C1), 128.70 (d, C2), 130.34 (s, C3). Selected IR (CsI, cm^{-1}): *ν* (N—H) 3423 cm^{-1} *ν* (C═N) 1627 cm^{-1} *ν* (C═C) 1465 cm^{-1} ν_{as} (P—CH) 1085 cm^{-1} *ν* (Ru—N) 529 cm^{-1} *ν* (Ru—P) 514 cm^{-1}, *ν* (Ru—Cl) 258 cm^{-1}. UV/visible spectrum [CH_2Cl_2; λ $_{max}$, nm (ε, M^{-1} cm^{-1})]: 298 (55828), 366 (23695), 480 (8615).

2.2.4. [RuCl(PPh$_3$)(Hdpa)(dmbipy)]Cl (4)

This compound was prepared by refluxing *cis*-[RuCl$_2$(PPh$_3$)$_2$(dmbipy)] (150 mg; 0.170 mmol) and Hdpa ligand (44 mg; 0.255 mmol) adopting the procedure used for **3**. Yield 124 mg (92%). Elemental analysis (%) Calc. for $C_{40}H_{36}Cl_2N_5PRu$: C 60.84; H 4.59; N 8.87 Found: C 61.05; H 4.34; N 8.86. NMR-^{31}P {^{1}H} (DMSO-d_6) [δ/ppm (multiplicity, assignment)] 41.7 (s, PPh$_3$). NMR-^{1}H (DMSO-d_6) [δ/ppm (multiplicity, integration, assignment, *J*/Hz, c.i.s)] 11.14 (s, 1H, NH, 1.51), 8.91 (s, 1H, H10′), 8.32 (d, 1H, H6′, ^3J = 5.6, 0.10), 8.20 (t, 2H, H13′/H13″, ^3J = 9.3), 8.00 (s, 1H, H10″), 7.86 (t, 1H, H8″, ^3J = 7.6, 0.22), 7.68 (t, 2H, H12′/H12″), 7.61–7,49 (m, 2H, H8′/H9″), 7.33 (t, 3H, H3, ^3J = 7.2), 7.23–7.10 (m, 7H, H2/H9′), 7.04–6.90 (m, 7H, H1/H6′), 6.64 (p, 2H, H7′/H7″, −0.22), 2.12 (s, 3H, CH$_3$″), 2.08 (s, 3H, CH$_3$′). NMR-^{13}C {^{1}H} (DMSO-d_6) [δ/ppm (multiplicity, assignment)] 157.23 (s, C6′), 148.59 (s, C6″), 117.86 (s, C7′), 118.40 (s, C7″), 138.61 (s, C8′), 139.00 (s, C8″), 115.59 (s, C9′), 113.73 (s, C9″), 154.18 (d, C10′/C10″), 18.09 (s, CH$_3$′), 18.51 (s, CH$_3$″), 136.87 (d, C12′/C12″),

122.64 (d, C13′/C13″), 133.41 (d, C1), 128.35 (d, C2), 129.96 (s, C3). Selected IR (CsI, cm^{-1}): ν (N—H) 3433 cm^{-1} ν (C=N) 1624 cm^{-1} ν (C=C) 1466 cm^{-1} ν_{as} (P—CH) 1089 cm^{-1} ν (Ru—N) 526 cm^{-1} ν (Ru—P) 516 cm^{-1}, ν (Ru—Cl) 252 cm^{-1}. UV/visible spectrum [CH_2Cl_2; λ_{max}, nm (ε, $M^{-1}\,cm^{-1}$)]: 304 (55348), 342 (shoulder).

2.2.5. [RuCl(PPh3)(Hdpa)(phen)]Cl (5)

The complex was prepared by refluxing *cis*-[$RuCl_2(PPh_3)_2$(phen)] (150 mg; 0.171 mmol) and Hdpa ligand (44 mg; 0.257 mmol) following the procedure used for **3**. Yield 113 mg (84%). Elemental analysis (%) Calc. for $C_{40}H_{32}Cl_2N_5PRu.^1/_{2.5}CH_2Cl_2$: C 59.20; H 4.03; N 8.54 found: C 59.09; H 4.04; N 8.24. NMR-^{31}P {^{1}H} (DMSO-d_6) [δ/ppm (multiplicity, assignment)] 43.1 (s, PPh_3). NMR-^{1}H (DMSO-d_6) [δ/ppm (multiplicity, integration, assignment, J/Hz, c.i.s)] 10.89 (s, 1H, NH, 1.26), 9.84 (d, 1H, H10′, ^3J = 5.3, 0.59), 9.11 (d, 1H, H10″, ^3J = 5.3, −0.14), 8.51 (d, 1H, H12′, ^3J = 8.2, −0.05), 8.40 (d, 1H, H12″, ^3J = 8.2, −0.17), 8.22 (d, 1H, H6′, ^3J = 5.8, 0.01), 8.01 (dd, 2H, H13′/H13″, ^3J = 8.9, −0.04), 7.89–7.80 (m, 2H, H8′/H11′), 7.70 (t, 1H, H11″, ^3J = 5.7, −0.16), 7.53 (d, 1H, H9′, ^3J = 8.1, −0.20), 7.43 (t, 1H, H8″, ^3J = 7.6, −0.21), 7.23–7.15 (m, 4H, H3/H6″), 7.02 (m, 7H, H2/H9″), 6.83 (t, 6H, H1), 6.61 (t, 1H, H7′, ^3J = 6.5, −0.24), 6.47 (t, 1H, H7″, ^3J = 6.5; −0.37). NMR-^{13}C {^{1}H} (DMSO-d_6) [δ/ppm (multiplicity, assignment)]. 157.96 (s, C6′), 148.72 (s, C6″), 117.89 (s, C7′), 118.42 (s, C7″), 138.59 (s, C8′), 138.98 (s, C8″), 115.38 (s, C9′), 113.42 (s, C9″), 155.06 (d, C10′), 156.51 (d, C10″), 125.65 (d, C11′), 124.61 (d, C11″), 135.42 (d, C12′), 125.69 (d, C12″), 127.60 (d, C13′/C13″), 133.18 (d, C1), 128.04 (d, C2), 129.95 (s, C3) Selected IR (CsI, cm^{-1}): ν (N—H) 3410 cm^{-1} ν (C=N) 1625 cm^{-1} ν (C=C) 1468 cm^{-1} ν_{as} (P—CH) 1089 cm^{-1} ν (Ru—N) 527 cm^{-1} ν (Ru—P) 510 cm^{-1}, ν (Ru—Cl) 256 cm^{-1}. UV/visible spectrum [CH_2Cl_2; λ_{max}, nm (ε, $M^{-1}\,cm^{-1}$)]: 272 (56713), 293 (shoulder), 434 (10105), 476 (shoulder).

2.2.6. [RuCl(PPh3)(Hdpa)(dphphen)]Cl (6)

This compound was prepared by refluxing *cis*-[$RuCl_2(PPh_3)_2$(dphphen)] (150 mg; 0.146 mmol) and Hdpa ligand (38 mg; 0.219 mmol) adopting the procedure used for **3**. Yield 121 mg (88%). Elemental analysis (%) Calc. for $C_{52}H_{40}Cl_2N_5PRu$: C 65.43; H 4.26; N 7.30 found: C 65.33; H 3.93; N 7.49. NMR-^{31}P {^{1}H} (DMSO-d_6) [δ/ppm (multiplicity, assignment)] 42.5 (s, PPh_3). NMR-^{1}H (DMSO-d_6) [δ/ppm (multiplicity, integration, assignment, J/Hz, c.i.s)] 11.03 (s, 1H, NH, 1.40), 9.93 (d, 1H, H10′, ^3J = 5.5), 9.15 (d, 1H, H10″, ^3J = 5.5), 8.22 (d, 1H, H6′, ^3J = 5.5, 0.01), 7.93–7.82 (m, 4H, H8′/H13′/H13″/H11′), 7.72–7.48 (m, 13H, H11″/H14′/H14″/H9′/H8″), 7.30–7.21 (m, 4H, H3/H6″), 7.19 (d, 1H, H9″, ^3J = 8.2, −0.55), 7.06 (t, 6H, H2, ^3J = 7.1), 6.89 (t, 6H, H1, ^3J = 8.5), 6.62 (p, 2H, H7′/H7″, −0.23). NMR-^{13}C {^{1}H} (DMSO-d_6) [δ/ppm (multiplicity, assignment)] 157.98 (s, C6′), 148.89 (s, C6″), 118.06 (s, C7′), 118.71 (s, C7″), 138.47 (s, C8′), 139.00 (s, C8″), 115.42 (s, C9′), 113.97 (s, C9″), 154.96 (d, C10′), 155.61 (d, C10″), 125.70 (d, C11′), 125.17 (d, C11″), 129.86 (d, C12′/C12″), 125.80 (d, C13′/C13″), 133.45 (d, C1), 128.03 (d, C2), 129.90 (s, C3). Selected IR (CsI, cm^{-1}): ν (N—H) 3427 cm^{-1} ν (C=N) 1623 cm^{-1} ν (C=C) 1468 cm^{-1} ν_{as} (P—CH) 1088 cm^{-1} ν (Ru—N) 530 cm^{-1} ν (Ru—P) 509 cm^{-1}, ν (Ru—Cl) 232 cm^{-1}. UV/visible spectrum [CH_2Cl_2; λ_{max}, nm (ε, $M^{-1}\,cm^{-1}$)]: 287 (49500), 328 (shoulder), 454 (8542), 493 (shoulder).

2.3. DNA interaction studies

A standard solution of calf thymus DNA (CT DNA) was prepared in the Tris–HCl buffer (5 mM Tris–HCl and 50 mM NaCl, pH 7.4, Tris = tris(hydroxymethyl)aminomethane). CT DNA solutions in the Tris-HCl buffer gave a ratio of UV absorbance at 260 and 280 nm of 1.8, indicating that the DNA was sufficiently free of protein. The DNA concentration was determined spectrophotometrically using the molar absorption coefficient of 6600 $mol^{-1}\,L\,cm^{-1}$ at 260 nm [26]. Initially, compounds **1**–**6** were solubilized in DMSO and diluted with Tris-HCl buffer afterwards. All the solutions of the compounds used in the experiments were prepared in the Tris–HCl buffer containing 5% DMSO.

2.4. Circular dichroism (CD)

CD spectra were registered on a Jasco J-810 spectropolarimetrer, equipped with a 450 W Xenon arc lamp. All experiments were done using a standard quartz cell of 10 mm path length. The CD measurements were performed from complex-DNA solutions in the Tris-HCl buffer (5% DMSO) at different molar ratios, [Complex]/[CT DNA] = 0.1, 0.2, 0.4, 0.6. The DNA concentration in the Tris-HCl buffer was kept constant (100 μM) in all samples. Complex-DNA solutions were incubated at 298 K for 18 h. After the incubation period, all CD spectra were recorded in the range of 240–300 nm. The spectra were expressed in terms of molar ellipticity.

2.5. Spectroscopic titrations

Absorption spectral titration experiments were performed by maintaining the constant concentration of the complexes and varying the CT DNA concentration. This was done by successive additions of CT DNA solution to solution of the compound in a quartz cell and recording the UV–Vis spectra after each addition of CT DNA. The binding constants were obtained using Eq. (1) [40]:

$$[DNA]/(\varepsilon_a - \varepsilon_f) = [DNA]/(\varepsilon_b - \varepsilon_f) + 1/[K_b(\varepsilon_b - \varepsilon_f)] \quad (1)$$

where [DNA] is the concentration of DNA in base pairs, ε_a, ε_f and ε_b are apparent-, free-, and bound-complex extinction coefficients, respectively. K_b is the equilibrium binding constant of the complex binding to DNA in M^{-1}.

2.6. Viscosity measurements

The viscosity assays were carried out using an Ostwald viscometer maintained at a constant temperature of 298 K in a thermostatic bath. First, 4 mL of complex-DNA solutions at different molar ratios, [Complex]/[CT DNA] = 0.08, 0.17, 0.25, 0.33, 0.42, 0.50, 0.58, 0.67, 0.75 were freshly prepared in the Tris-HCl buffer (5% DMSO) prior to use. The DNA concentration in the Tris-HCl buffer was kept constant (98 μM) in all samples. Afterwards, the flow times of the solutions on the Ostwald viscometer were measured using a digital stopwatch 5 times, taking the average flow time into consideration. The relative viscosity of DNA in the absence (η^o) and presence of complexes (η) was calculated from Eq. (2): $\eta/\eta^o = (t - t_o)/(t_{DNA} - t_o)$, where t_o and t_{DNA} are the flow time of the buffer and DNA solution alone, respectively, while t is the flow time of DNA solution in the presence of the ruthenium compounds [41a]. Data are presented as $(\eta/\eta^0)^{1/3}$ versus the ratio [complex]/[DNA].

2.7. Agarose gel electrophoresis studies

pTZ57RT plasmid (100 mM) in buffer Tris-HCl buffer was treated with each compound at different molar ratios. The different ratios of complex/plasmid were 0 (control); 0.5; 1.0; 2.0. The solutions were incubated at 310 K for 18 h, and then 5 μL of each sample were analyzed by electrophoresis for 90 min at 100 V on a 1% agarose gel in the TAE buffer [0.45 M Tris–HCl, 0.45 M acetic acid, 10 mM ethylenediaminetetraacetic acid (EDTA)]. The gels were stained with 1 μg mL^{-1} ethidium bromide under UV light and photographed using a ChemiDoc MP. Samples of free DNA and DNA/DMSO were used as controls.

2.8. Partition coefficient determination

Lipophilicity, commonly expressed log P (the partition coefficient of a compound in two immiscible phases, as water and n-octanol). Water-octanol partition coefficients were determined using the shake flask

method [41b]. The determination was carried out at in a mixture of equal volumes of water and n-octanol, and continuously shaking for 18 h at room temperature. The concentrations of complexes in n-octanol and water were measured spectrophotometrically in order to determine values of $P = [compound]_{n\text{-}octanol}/[compound]_{water}$.

2.9. Fluorescence quenching experiments

The protein binding study was performed by a tryptophan fluorescence quenching experiment using human serum albumin (HSA). The extinction of emission intensity of the tryptophan residue at 305 nm was monitored using the compounds as suppressors. The fluorescence measurements were performed using compound-HSA solutions in the Tris-HCl buffer (5% DMSO) at different molar ratios, [Compound]/[HSA] = 0 (control), 1, 2, 3, 4, 5, 6, 7. The HSA concentration in the Tris-HCl buffer was kept constant (5 μM) in all samples. Emission spectra were recorded between 300 and 500 nm upon excitation at 270 nm. Fluorescence spectra were registered on a SpectraMax M3 at different temperatures (295 and 310 K) and in triplicate. All experiments were conducted using an opaque 96-well plate. The fluorescence data were analyzed using the Stern-Volmer Eq. (2) [42]:

$$F_0/F = 1 + k_q t_0 [Q] = 1 + K_{sv}[Q] \quad (2)$$

where F_0 and F are fluorescence intensities in the absence and presence of the quencher, respectively. K_{sv} is the Stern-Volmer quenching constant. k_q is the biomolecular quenching constant and t_0 is the average lifetime of fluorophore in the absence of the quencher; [Q] is the concentration of the quencher. The K_{sv} constant was obtained from the slope of the linear regression of F_0/F versus [compound] plot. The k_q constant was calculated by the ratio between K_{sv} and t_0 ($k_q = K_{sv}/t_0$).

The binding constant (K_b) and the number of binding sites (n) for the interactions of HSA and compounds were determined by Eq. (3).

$$\log [(F_0 - F)/F] = \log K_b + n \log[Q] \quad (3)$$

The thermodynamic parameters of the intermolecular forces involved in the interactions between HSA and compounds were calculated using the modified van't Hoff equation, Eq. (4) [43]:

$$\ln K = -\Delta H/RT + \Delta S/R \quad (4)$$

where K is analogous to the Stern-Volmer quenching constant at the corresponding temperature (T); the temperatures used were 295 and 310 K; R = gas constant; ΔH = enthalpy change and ΔS = entropy change. The values were obtained from the slope of the linear regression of ln K versus 1/T plot. Furthermore, the free energy change (ΔG) was calculated using Eq. (5) [43].

$$\Delta G = -RT \ln K = \Delta H - T\Delta S \quad (5)$$

2.10. Cell proliferation

In vitro cytotoxicity assays on cultured human tumor cell lines represent the standard method for the initial screening of antitumor agents. Thus, as a first step to assess their pharmacological properties, the ruthenium complexes were assayed using the human breast tumor cell line MDA-MB-231 (ATCC HTB-26) and the Chinese hamster lung fibroblast non-tumor cell line V79–4 (ATCC CCL-93). The cells were routinely maintained in Dulbecco's Modified Eagle's medium (DMEM) supplemented with 10% fetal bovine serum (FBS), L-glutamine (2 mM), penicillin (100 UI mL^{-1}) and streptomycin (100 mg mL^{-1}) at 310 K in a humidified 5% CO_2 atmosphere.

Briefly, all cell lines were prepared at a concentration of 1.5×10^4 cells/150 μL, in complete medium (with 10% FBS), and plated on sterile 96 well plates for 24 h at 310 K in a humidified 5% CO_2 atmosphere. The complexes were added to the wells at different concentrations and incubated for 48 h under the same conditions as described above. The cell proliferation assay was performed compared to the wells where the vehicle (0.5% DMSO) was added instead of the tested compounds. After incubation, the culture medium of each well was removed and a solution containing MTT (0.5 mg ml^{-1}) was added (100 μL/well) [44]. The plates were then kept at 310 K for 4 h and the formed crystals were dissolved in isopropyl alcohol. The absorbance was read on an ELISA plate reader at a wavelength of 595 nm and the IC_{50} (concentration of compound that induced 50% of cell death) value were determined.

2.11. Cell morphology

MDA-MB-231 growing cells were harvested, counted and seeded at 8×10^4 cells/well in 12-well plates. The cells were allowed to grow at 310 K in a humidified 5% CO_2 atmosphere overnight and then, treated or not (control) with 0.2, 2.0 and 20.0 μM of compound **6** for 0, 12, 24, 36 and 48 h. Cell morphology was examined under an inverted microscope at 100× magnification.

3. Results and discussion

3.1. Synthesis and characterization of the complexes

The $[RuCl(PPh_3)(Hdpa)_2]Cl$ (**1**) complex was prepared from the reaction of $[RuCl_2(PPh_3)_3]$ precursor with 2,2′-dipyridylamine ligand, in dichloromethane. The cationic ruthenium (II) complexes $[RuCl(PPh_3)(Hdpa)(N{-}N)]Cl$ [N-N: en (**2**), bipy (**3**), dmbipy (**4**), phen (**5**) and dphphen (**6**)] were synthesized by treating the respective $[RuCl_2(PPh_3)_2(N{-}N)]$ precursor with the 2,2′-dipyridylamine, in 1:1 dichloromethane/methanol solution, as shown in Scheme 1.

Reagents and conditions: (a) PPh_3 (5 equivalents), methanol, reflux; (b) Hdpa (2 equivalents), CH_2Cl_2, agitation; (c) en (1 equivalent), CH_2Cl_2, agitation; (d) Hdpa (1 equivalent), CH_2Cl_2, agitation; (e) N—N (1 equivalent; N-N = bipy, dmbipy, phen or dphphen), CH_2Cl_2, agitation; (f) Hdpa (1.5 equivalent), dichloromethane/methanol (1:1), reflux.

All complexes were characterized by 1D (^{31}P $\{^1H\}$, ^1H, ^{13}C $\{^1H\}$) and 2D (^1H — ^1H COSY; ^1H — ^{13}C $\{^1H\}$ HSQC) NMR, UV and IR spectroscopy, cyclic voltammetry, CHN analyses, molar conductance and X-ray crystallography, for complexes **1**, **2** and **4**. The CHN analyses of the complexes are according to the proposed formula. The molar conductivity values of 1 mmol L^{-1} solutions of complexes **1**–**6** in dimethyl sulfoxide are in the range of 38–46 S cm^2 mol^{-1}, indicating that the complexes are 1:1 electrolytes [45].

3.2. NMR spectroscopy

The $^{31}P\{^1H\}$ NMR spectra (in the Supporting Information) of complexes in DMSO-d_6 present a singlet (A spin system). The chemical shifts are consistent with a structure in which the phosphorus atom is *trans* to Ru—N_{py} bond for **1** and **3**–**6**, whereas for **2** it is *trans* to Ru—NH_2 [37].

The assignments of ^1H spectra (see Figures in the Supporting Information) of the compounds are summarized in the Experimental section. The resonances of the compounds show inequivalent aromatic rings for the Hdpa ligand, as well as from the diimines. In all complexes, the NH group (Hdpa ligand) resonance shows a great variation in the chemical shift toward the region of higher frequencies of the ^1H NMR spectrum after the ligand coordination to the metal center.

3.3. X-ray crystallography

The crystal structures of complexes **1**, **2** and **4** were determined by X-ray crystallography. The ORTEP diagrams are shown in Fig. 1, while the selected bond lengths and angles are reported in Table 2. In all three structures, the cationic complexes show a distorted octahedral coordination geometry around the Ru(II) center.

In all structures, the dipyridylamine ligand is chelated to the Ru(II) by pyridinic-N atoms, with the free group NH pointed out from the

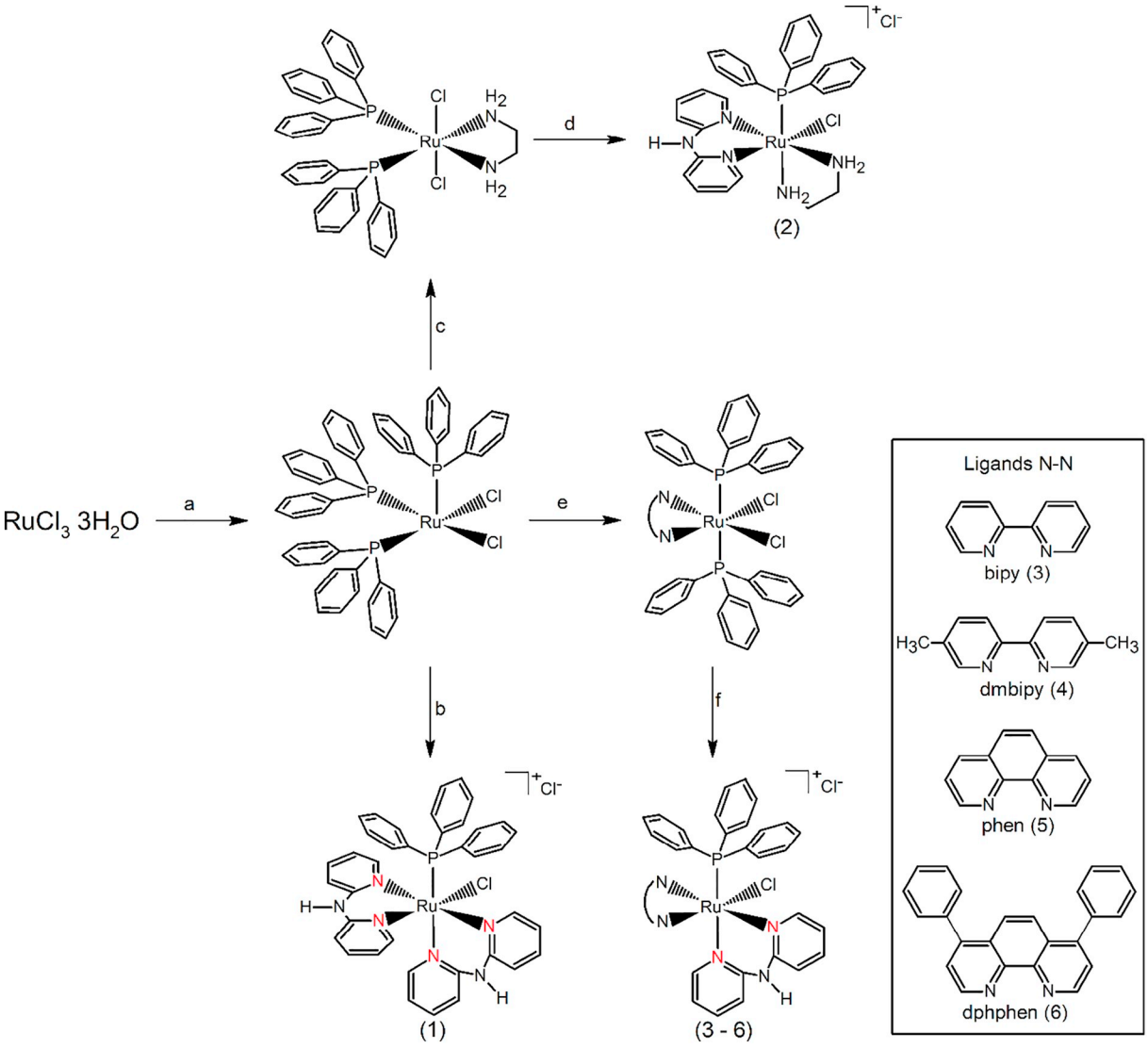

Scheme 1. Synthetic pathways for the preparation of complexes **1**–**6**.

rings. In compound **4**, the dmbipy ligand is coordinated in the equatorial plane, whereas the Hdpa ligand occupies a position *trans* to the PPh_3 ligand, and another position in the equatorial plane, *trans* to N1(dmbipy).

The Ru−N bond lengths [2.157 (3) and 2.156 (3) Å] are observed in the complex with the 1,2-diaminoethane ligand, since it is typical for Ru—Nsp_3 distances. The Ru—N_{en} distances are longer than those of the Ru−N (diimine, Hdpa) bond lengths. This trend is consistent with the characteristic moderate π acceptor of the diimine ligand, while the en ligand is only a pure σ-donor. In complex **4**, the Ru—N coordination bond lengths of the dmbipy ligand are shorter than those Ru—N(Hdpa) distances. This finding is consistent with the better π acceptor ability of the dmbipy ligand, compared to the Hdpa ligand [27]. The Ru−P bond

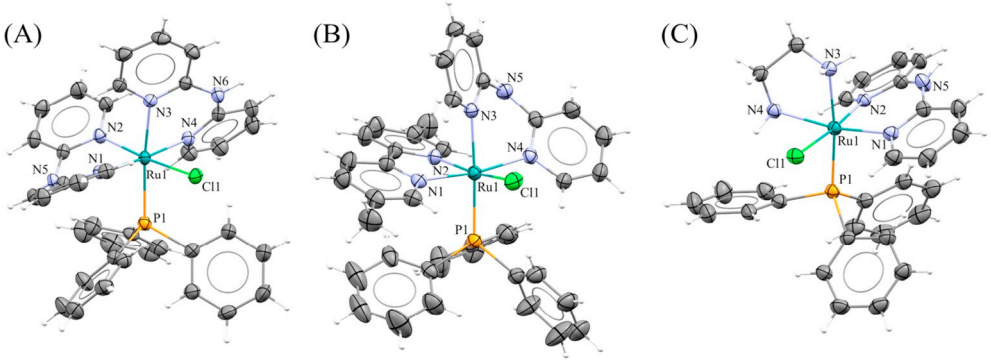

Fig. 1. ORTEP view of compounds $[RuCl(PPh_3)(Hdpa)_2]Cl$ (A), $[RuCl(PPh_3)(Hdpa)(dmbipy)]PF_6$ (B) and $[RuCl(PPh_3)(Hdpa)(en)]PF_6$ (C), showing the atom labels and the 30% probability ellipsoids. The anions are omitted for clarity.

Table 2
Selected bond lengths (Å) and angles (°) for complexes **1**, **2** and **4**.

Compound	Bond lengths (Å)			Compound	Bond angles (°)		
	1	2	4		1	2	4
Ru(1)–Cl(1)	2.362(7)	2.299(1)	2.344(1)	P(1)–Ru(1)–Cl(1)	88.89(3)	89.18(4)	99.32(3)
Ru(1)–P(1)	2.434(8)	2.430(1)	2.425(1)	P(1)–Ru(1)–N(3)	173.12(7)	173.68(9)	175.97(9)
Ru(1)–N(3)	2.123(2)	2.157(3)	2.132(3)	Cl(1)–Ru(1)–N(2)	172.88(9)	174.7(1)	168.20(9)
Ru(1)–N(2)	2.077(2)	2.083(3)	2.061(4)	N(1)–Ru(1)–N(4)	175.35(9)	165.7(1)	171.6(1)
Ru(1)–N(4)	2.098(2)	2.156(3)	2.110(3)	N(1)–Ru(1)–N(2)	87.11(9)	90.5(1)	78.8(1)
Ru(1)–N(1)	2.097(2)	2.107(4)	2.047(3)	N(3)–Ru(1)–N(4)	85.28(9)	80.3(1)	84.1(1)

lengths, in all compounds, are influenced by the nature of the ligand in the position *trans* to it: in complex **2**, the Ru—P bond length *trans* to NH_2 (en ligand) is significantly the shortest value compared to those *trans* to the Hdpa ligand, in complexes **1** and **4**.

The hydrogen bonds in the crystal structures of the complexes involve the –NH– groups of the Hdpa ligand acting as hydrogen bonds where the chlorido ligand acts as a hydrogen bond acceptor. The intermolecular distance of 2.25 Å between H….Cl is indicative of strong hydrogen bonds [46]. Other hydrogen bonds, defined by a hydrogen acceptor distance shorter than the sum of van der Waals radii, are formed between C—H donors and the chlorido ligand. Relatively long intermolecular distances suggest that they may be classified as weak interactions [46]. Considering these observations in the crystal self-assembly, it can be expected that the –NH– group in the Hdpa ligand may also perform hydrogen bonds and interactions in aqueous medium with biomolecules.

3.4. UV/Vis spectroscopy studies

In the UV region, the spectrum of each complex shows a strong absorption band centered at about 300 nm, assigned to the intraligand-centered π—π* type transition, also present in the spectra of the free ligands. The metal to ligand charge transfer (MLCT) transitions from Ru (dπ) to the ligand (π) for complexes **1–6,** which appear in the region of the typical spectra of ruthenium compounds, where the metal is coordinated to polypyridyl ligands. In the region of 350–470 nm, the complexes exhibit lower-energy absorption bands attributed to MLCT transitions π (Hdpa) ← dπ(Ru) and π (diimine) ← dπ(Ru) [47a,48].

3.5. Electrochemistry

The electrochemical behavior of compounds **1–6,** in dichloromethane solutions, was studied by cyclic voltammetry (in the Supporting Information). All the complexes showed similar electrochemical behavior, where the CVs of the complexes exhibit a redox couple (I) with half-wave potential ($E_{½}$) values in the range of 0.7–1.1 V vs. Ag/AgCl (Table 3), attributed to the transfer of one electron of the Ru(II)/Ru(III) couple. In addition, the peak potentials (E_{pa} and E_{pa}) are nearly scan-rate independent and the ratios of the cathodic (I_{pc}) to anodic (I_{pa}) peak currents are close to one, suggesting that the redox processes are quasi-reversible type.

The Ru(II) oxidation state is stabilized when the PPh_3 and chlorido ligand are replaced by the Hdpa ligand (also π-acceptor), which is consistent with enhanced π delocalization. The oxidation potential of compound **1** is low when compared to those possessing the diimine co-ligands, compounds **3–6**. This is an effect of its higher energy π* orbitals and the stronger σ-donating and less π-accepting ability of Hdpa ligand, when compared to other diimine ligands [27,47a]. Similarly, complex **2** showed the lowest $E_{1/2}$ among all the complexes, which is attributed to the influence pure σ-donor character of the diaminoethane ligand, which results in a more electro-rich metal center.

The difference of the oxidation potentials of the complexes, with the same composition and structure, can be analyzed using the pKa values of the co-ligands, as shown in Fig. S7 (Supporting Information). It can be observed that the compounds with the diimines (bipy, dmbipy, phen and dphphen), which have lower pKa than the en ligand, have higher oxidation potentials than the [RuCl(PPh_3)(Hdpa)(en)]Cl (2) complex.

In addition, all complexes also exhibit one irreversible oxidation wave (E_{pa3}) with values falling in the range of 1.29–1.34 V vs. Ag/AgCl, which is attributed to oxidation of the -NH- of Hdpa ligands. The irreversible oxidation process is also observed in the free Hdpa ligand.

3.6. Chemical behavior of the complexes in aqueous solution

Contrary to that commonly observed for ruthenium/phosphine complexes, the new compound **2** is well soluble in water, while compound **1** is only slightly soluble in this solvent. Complexes **3–6** are insoluble in water. All the complexes are soluble and stable in solvents such as DMSO, *N*,*N*-dimethylformamide and chlorinated solvents, and are also soluble in mixture of 1%:99% DMSO: H_2O, at micromolar concentrations (relevant for biological studies).

The stability of the complexes **1–6** in D_2O/DMSO (50:50) mixture was investigated by $^{31}P\{^1H\}$ NMR spectroscopy. Compounds **1** and **3–6** are stable in the tested solutions, where their NMR spectra remained unchanged for at least 96 h. Contrary, immediately after the solubilization of compound **2** in D_2O/DMSO mixture, a new singlet at 53 ppm was observed in its $^{31}P\{^1H\}$ spectrum, Fig. S28 (Supporting Information), which increased at the expense of the signal at 64 ppm. The new singlet can attribute to the formation of the aqua species [Ru(OH_2)(PPh_3)(Hdpa)(en)]$^{2+}$ (**2aq**) by replacing the chlorido ligand from the coordination sphere of the ruthenium center. The species, in solution, reached an equilibrium, within about 45 min after dissolution of the complex, with a 40:60 ratio between **2** and **2aq**. The lability of the

Table 3
Electrochemical data of phosphine ruthenium complexes. TBAP (0.1 M); CH_2Cl_2; Ag/AgCl; scan rate of 100 mVs^{-1}.

Compound	E_{pa1}/mV	E_{pc2}/mV	ΔE_p/mV	$E_{1/2}$/mV	I_{pa1}/I_{pc2}	E_{pa3}/mV	p*Ka*[a]
1	813	727	86	770	1.03	1327	6.48
2	767	688	79	728	1.01	1226	9.98
3	984	821	163	902	0.99	1336	4.33
4	954	852	102	903	1.12	1290	4.58
5	1031	906	125	969	1.03	1318	4.27
6	1010	912	98	961	1.05	1292	4.29

[a] p*Ka* of the co-ligands: Hdpa [47b], en [47c], bipy [47d], dmbipy [47d], phen [47b], dphphen [47b].

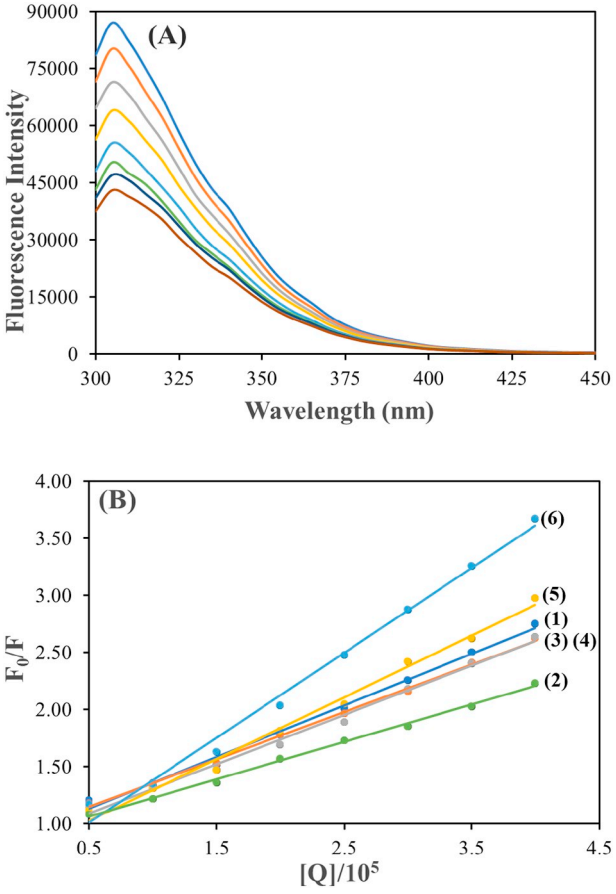

Fig. 2. (A) Fluorescence quenching spectra of HSA in the absence and presence of compound 6 at different [compound]/[HSA] ratios (a = 0.5; b = 1; c = 2; d = 3; e = 4; f = 5; g = 6; h = 7, with the excitation wavelength at 270 nm, at 310 K in Tris-HCl buffer. Arrow indicates the increase of quencher concentration. (B) Stern-Volmer plots for HSA fluorescence quenching observed with compounds 1–6.

Cl^- ligand in complex **2** is attributed to the influence of the σ-donor en ligand, compared to the σ-donor and π-acceptor diimine ligands in compounds **1** and **3–6,** which do not undergo hydrolysis of the complex [30].

3.7. HSA binding study by fluorescence quenching

HSA is the most abundant protein in plasma and its principal function is to transport metabolites, playing an important role in the drug distribution and efficacy since it increases the solubility of hydrophobic drugs in the plasma. Currently, an important study in the development of novel drug candidates is to investigate their binding affinity with human serum albumin, which is an important step in the pharmacological characterization [42,49]. The interaction of ruthenium phosphine compounds **1–6** with HSA was studied by tryptophan fluorescence quenching.

Fig. 2A shows significant fluorescence quenching of HSA in the presence of compound **6** (Supporting Information). A substantial decrease in HSA fluorescence intensity was observed with the increasing amounts of the complexes in the solution, and in the higher molar ratio of compound/protein (r = 7) the fluorescence intensity of HSA was approximately 49–33% of the initial value. The quenching of HSA fluorescence clearly indicates that the interaction of compounds causes conformational change in the microenvironment of the Trp21p residue, located in the subdomain IIA.

The fluorescence quenching of HSA, in the presence of the complexes, was measured at different temperatures, in order to ascertain the fluorescence quenching mechanism. The mechanisms of quenching are usually classified as dynamic quenching and static quenching, which can be distinguished examining their temperature dependence, or by the lifetime of fluorophore measurements [43]. The K_{sv} constants (Table 4) were determined using the Stern-Volmer equation. The linearity of the Stern-Volmer plots (Fig. 2B) suggests the involvement of only one type of quenching [42]. The decrease in the K_{sv} values with an increase in temperature indicates the existence of static quenching due to the formation of the fluorophore-quencher intermediate in the ground state.

The bimolecular quenching constants (k_q) were also determined using the Stern-Volmer equation and assuming t_0 = 6 ns for HSA [50]. The maximal value resulting for dynamic quenching of biopolymers is $2.0 \times 10^{10}\,M^{-1}\,s^{-1}$ [51]. The k_q constants were higher than

Table 4
Stern-Volmer quenching constant (K_{SV}), biomolecular quenching rate constant (k_q), binding constant (K_b), number of binding sites (n) and the thermodynamic parameters for the compound-HSA system at different temperatures.

Temperature	K_{sv} ($\times 10^4\,M^{-1}$)	k_q ($\times 10^{12}\,M^{-1}\,s^{-1}$)	K_b ($\times 10^5\,M^{-1}$)	N	ΔH° (KJ mol^{-1})	ΔS° (KJ $mol^{-1}\,K^{-1}$)	ΔG° (J $mol^{-1}\,K^{-1}$)
Compound 1							
295	4.80 ± 0.06	8.01 ± 0.15	1.54 ± 0.80	1.12	55.72	291.44	−31.12
310	4.73 ± 0.04	7.88 ± 0.08	4.75 ± 1.10				−34.62
Compound 2							
295	3.38 ± 0.08	5.63 ± 0.13	04.44 ± 0.31	1.26	77.34	374.86	−34.36
310	3.28 ± 0.07	5.47 ± 0.16	21.73 ± 4.27				−38.86
Compound 3							
295	4.28 ± 0.03	7.13 ± 0.07	02.94 ± 0.15	1.10	59.66	310.48	−32.86
310	4.26 ± 0.12	7.10 ± 0.20	10.07 ± 0.11				−36.59
Compound 4							
295	4.81 ± 0.02	8.01 ± 0.05	04.67 ± 0.47	1.22	49.08	277.70	−33.68
310	4.47 ± 0.11	7.44 ± 0.18	12.46 ± 0.29				−37.01
Compound 5							
295	5.66 ± 0.01	9.44 ± 0.03	14.31 ± 0.27	1.33	65.12	342.42	−36.92
310	5.14 ± 0.07	8.57 ± 0.11	54.53 ± 15.13				−41.03
Compound 6							
295	9.46 ± 0.15	15.76 ± 0.36	90.35 ± 0.46	1.47	51.14	309.50	−41.09
310	8.85 ± 0.22	14.75 ± 0.37	255.8 ± 25.28				−44.80

$2.0 \times 10^{10}\,M^{-1}\,s^{-1}$ for all complexes. The k_q values decrease when the temperature is increased due to the stability of the fluorophore, while the quencher complex is lowered at higher temperatures. Therefore, the results suggest that the fluorescence quenching mechanism of HSA in the interaction with the compounds is static.

The fluorescence data were treated using the modified Stern-Volmer equation to determine the binding constants (K_b) and number of binding sites (n) for the interaction of HSA with the complexes (Table 4). From the binding constants (K_b), the thermodynamic parameters (Table 4) were calculated using the Van't Hoff thermodynamic equation [43].

The signs and magnitudes of thermodynamic parameters were analyzed to evaluate the main intermolecular forces involved in the interaction between the compounds and HSA. According to Ross and Subramanian [43], when $\Delta H > 0$ and $\Delta S > 0$ it implies that the main force is due to hydrophobic interactions; $\Delta H < 0$ and $\Delta S < 0$ reflect van der Waals force or hydrogen bond formation; $\Delta H < 0$ and $\Delta S > 0$ imply that the main force is due to electrostatic interactions. The negative values of ΔG reveals that the interaction processes between all compounds and HSA are spontaneous. All complexes present positive ΔH and ΔS values, which is indicative that their insertions in the protein framework are determined by hydrophobic interactions.

The number of binding sites between HSA and the ruthenium complexes is approximately equal to 1. The relatively high K_b values for the complexes are reflected moderate to strong interactions with the HSA. The preference of Ru-phosphine-compounds to bind the subdomain IIA of the HSA [23c,52] was shown. The new complexes 1–6 have a hydrophobic moiety, mainly by the presence of PPh_3 moiety. Thus, the high binding affinity of the compounds to HSA can be explained by interactions of the compounds by hydrophobic cavity of subdomain IIA of the biomolecule. Hence, transporting compounds **1**–6 in human plasma would be performed by HSA, and thus the absorption and distribution to various tissues can be feasible [49].

The compounds containing phen **(5)** and dphphen **(6)** ligands presented the strongest interactions with HSA among the **1–6** complexes. Even though the hydrophobic interaction plays a major role in the binding forces, other types of interactions, such as π-π interactions through the aromatic rings and size of diimine ligands, may play a further role in the binding affinity between HSA and compounds 5 and 6 [52–56].

3.8. DNA binding studies

3.8.1. Viscosity studies

The CT DNA viscosity studies are regarded as one of the most effective methods and least ambiguous to evaluate the binding mode between DNA and complexes, in solution [41a,57,58]. The viscosity measurements are sensitive to length changes of the DNA, and it is known that the DNA viscosity enhances significantly due to complete or partial intercalation of drugs into its base pairs [58]. In contrast, the electrostatic or groove interaction between the compounds and DNA cause a less significant change in the viscosity of the biomolecule [21]. The covalent binding of the complex/DNA can cause kinks or bends in the DNA double helix, decreasing its viscosity [23e]. The effects of complexes **1–6** on the relative CT-DNA viscosity are shown in Fig. 3. The relative viscosity of DNA solutions did not show any significant changes upon adding complexes **1–5**. These results suggest that compounds **1–5** do not cause conformational changes in the DNA double helix, which is consistent with weak DNA reversible binding. In contrast, when increasing the concentration of compound [RuCl(PPh_3)(Hdpa)(dphphen)]Cl **(6)**, the relative viscosity of the DNA solutions gradually decreased. This behavior can be associated with two types of interactions: (a) Covalent binding between the complex-DNA. Indeed, studies on reactivity followed by NMR showed that compound **6** does not react with guanosine-5′-monophosphate (5′-GMP) and its ability to bind DNA is unlikely. (b) Cooperative surface interaction complex-DNA by the grooves. Thus, the interaction of complex **6,** by covalent binding with the DNA is not probable because this compound is very stable in solution, but its interaction through the DNA grooves is more viable to happen, since the dphphen ligand has phenyl rings, with torsional freedom allowing them to twist and become isohelical with the DNA groove. As reported by GILL et al. [13], the DNA groove binding is also dependent on a combination of van der Waals and electrostatic interactions and hydrogen bonding that has a key role of stabilizing the complex-DNA groove interaction. Hence, the possible hydrogen bonding of the NH-group of Hdpa ligand with the DNA may play a further role in stabilizing the interaction of complex 6 with the DNA groove binding [13,27,57].

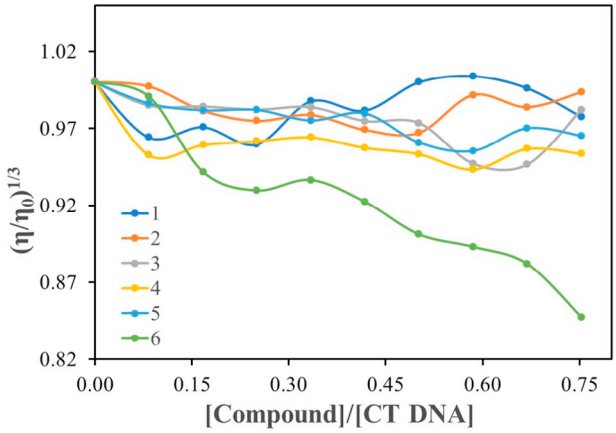

Fig. 3. Effect of increasing concentration of phosphine Ru(II) complexes **1–6** on the relative viscosity of CT DNA; [DNA] = 98 μM. The lines are guides for the lecture of the points.

3.8.2. Electrophoretic mobility of the complexes 1–6 in gel agarose

The ability of compounds **1–6** to modify the tertiary structure of DNA was also examined by monitoring changes in the electrophoretic mobility of pTZ57RT plasmid in gel agarose [59]. The electrophoretograms of the pTZ57RT plasmid treated with different concentrations of the compounds are given in Fig. 4. The degree of folding the forms of plasmid DNA treated with compounds **1–5** showed no significant changes, which is very similar to the migration pattern of the untreated DNA. In contrast, compound 6 induced significant changes in the electrophoretic mobility of the plasmid forms. The amount of plasmid forms decreases when the concentration of compound **6** reaches the higher molar ratio of compound/pTZ57RT (r = 2), containing no band corresponding to any form of the biomolecule. These changes in the migration pattern of the DNA bands may be due to several factors. The two most common are the fragmentation of the DNA duplex helix by covalent binding of the compound to DNA [23e] or by quenching ethidium bromide (EtBr) emission caused when the EtBr is expelled out of the DNA plasmid through intercalation of the compounds between the DNA base pairs. However, on some occasions, as already described in the literature, compounds that are very closely associated with the DNA groove structure, leading to substantial conformational changes, are capable of expelling the EtBr from the DNA plasmid. This is in accordance with other reported complexes with similar behavior [23d].

3.8.3. Circular dichroism studies

The possible effects of compounds **1–6** in the DNA secondary structures during the binding process were investigated by the circular dichroism (CD) technique. The CD spectrum of the CT-DNA in Trizma-HCl buffer shows a positive band with a maximum at 275 nm due to the base stacking, and a negative band with a minimum at 240 nm due to the right-handed ellipticity, characteristic of the B-DNA conformation

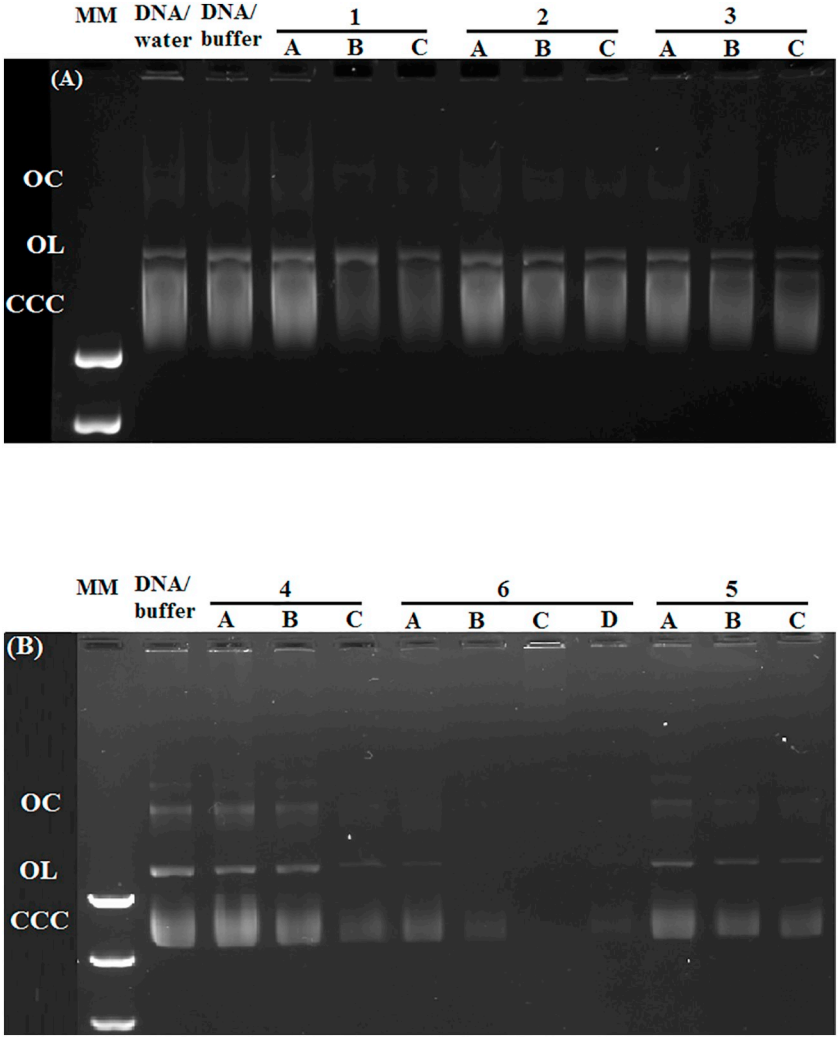

Fig. 4. Electrophoresis mobility shift assays of plasmid pTZ57RT for compounds **1–6** DNA/water refers to untreated plasmid pTZRT57 in water; DNA/buffer refers to untreated plasmid in Tris-HCl buffer; A, B, and C correspond to [compound]/[plasmid] ratios of 0.5; 1.0; 1.5, respectively (D corresponds to 1.25).

[58,60]. Alterations in the CD signals can be assigned to modifications in the secondary structures of DNA from the DNA-complex interactions [61]. In the CD spectra of CT-DNA (Fig. 5, CD spectra of compounds **5** and **6**; see Supporting Information, CD spectra of **1–4**) in the presence of complexes **1–5,** minor changes are observed of the bands compared with untreated CT-DNA, with a slight decrease in the intensity of the negative band and no alteration in the positive region, and without a shift in the maximum of the absorption bands. These observations indicate that the DNA binding to complexes **1–5** does not induce conformational changes in the DNA secondary structures, suggesting the existence of weak interaction between DNA/complexes [60,62]. In contrast, the bigger change in CT-DNA was observed for compound **6.** In this case, the intensities of both the positive and negative bands decreased, indicating that the interaction of compound **6** with the DNA molecule causes disturbances in the wavelength and ellipticity of the DNA (compared to free DNA). This type of alteration in the profile of the CD spectrum of CT-DNA is indicative of conformational changes caused by a non-intercalative mode of binding of the compound to the biomolecule and offers support that the complex is binding to the groove of the DNA [62].

3.8.4. DNA binding: electronic absorption titrations

The mode and strength of binding between the complexes and CT-DNA are usually studied by Ultraviolet-visible spectroscopy, by monitoring changes in the UV spectra of the complexes upon adding CT-DNA [11]. The absorption spectra of compound **6** in the absence and presence of CT-DNA are given in Fig. 6. After successively adding the CT-DNA, the intensities of the intraligand (IL) bands of complexes **1–6** exhibit uniform hypochromism ($\Delta\varepsilon$) of 7–16%, with a red shift of 2–4 nm, clearly revealing that these complexes bind to DNA by a non-intercalative mode [40].

In order to elucidate the binding strength of the compounds to DNA, the intrinsic binding constant (Table 5) was determined by changes of absorbance at the IL band. The constants exhibited by synthesized complexes are less than those reported for DNA classical intercalators, such as $[Ru(bipy)_2(dppz)]^{2+}$ and $[Ru(phen)_2(dppz)]^{2+}$ (dppz = dipyridophenazine) [18], but similar for the compounds with electrostatic interactions through the phosphate backbone of DNA and groove of DNA, such as $[Ru(bpy)_3]^{2+}$ [63,64]. The compounds exhibit similar intrinsic binding constants, however compound **6** stands out with the highest K_b and hypochromism. Thus, the highest complex-6/DNA interaction is in agreement with other interaction data evaluated here.

3.8.5. DNA binding discussion

Firstly, the experimental results for the complex/DNA binding mode clearly showed that all the six compounds present non-intercalating interactions. Compounds **1–5** do not lead to any conformation change in the structure of the DNA, and their binding constants are approximately $1.0 \times 10^4\,M^{-1}$, which is a typical behavior of weak reversible DNA-complex interaction, suggesting that the interaction of compounds

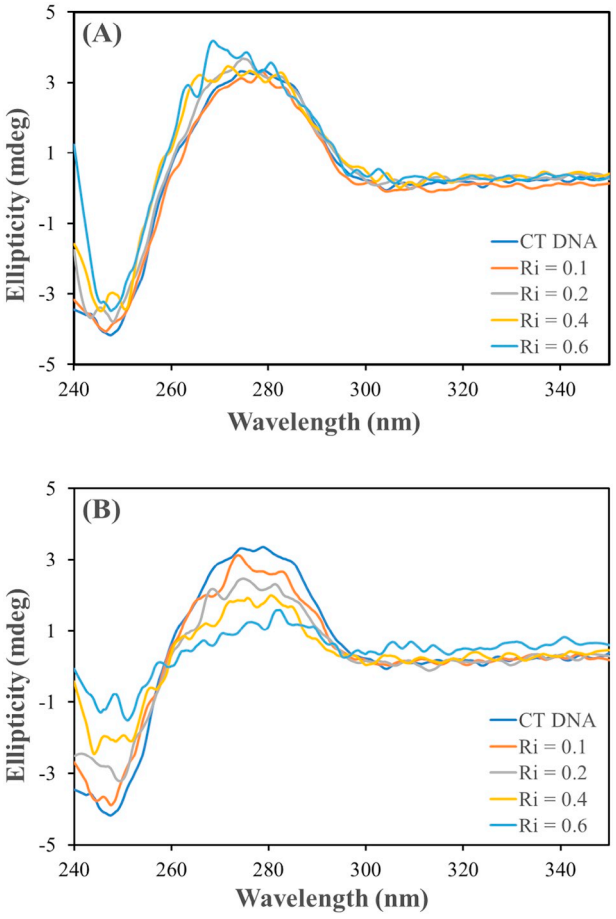

Fig. 5. Circular dichroism (CD) spectra of CT DNA in the absence and presence of compounds **5** (A) and 6 (**B**) at different [compounds]/[DNA] ratios; [DNA] = 50 μM.

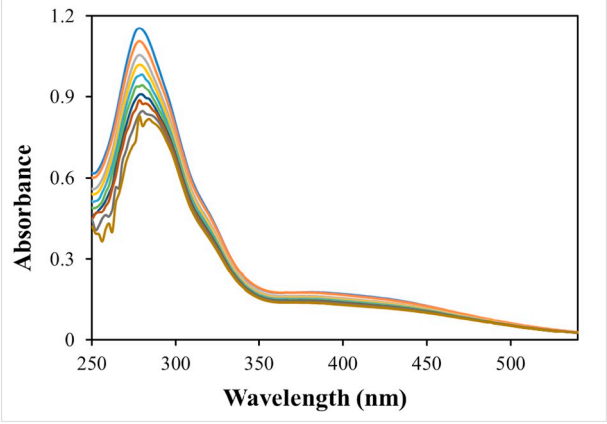

Fig. 6. Spectrophotometric titration spectra of compound **6** with CT-DNA. [Complex] = 1.03×10^{-5} mol L^{-1}, [DNA] = 0–5.43×10^{-4} mol L^{-1}.

1–5 with DNA are electrostatic attractions between the cationic compounds and the anionic phosphate backbone of the DNA. NMR studies have demonstrated that compound **2** undergoes partial hydrolysis of the Cl^- ligand in aqueous media, however in the Tris-HCl buffer the hydrolysis is inhibited due to high concentration of NaCl (50 mM). In the binding studies a behavior of non-covalent interaction was observed, indicating that the species in aqueous solution are not capable of covalently binding to DNA (as DNA bases).

Moreover, our studies demonstrated that the nature of the ligand

Table 5
Binding constants for the interactions between the ruthenium complexes and CT DNA.

Compound	λ (nm)	Δε (%)	K_b ($\times 10^4\ M^{-1}$)
1	288	11.3	3.8 ± 0.3
2	297	7.4	0.9 ± 0.2
3	305	9.1	1.2 ± 0.6
4	271	12.7	2.6 ± 0.9
5	287	11.9	1.3 ± 0.7
6	298	14.8	4.1 ± 0.5

N—N is a feature that can modulate the DNA binding mode with the compounds. The interaction assays show that the compound **6**-dphphen causes modifications in the secondary and tertiary structures of DNA and exhibits the highest DNA binding affinity among compounds. The results suggest that compound **6** acts by surface interactions within DNA grooves. The structures of the **5**-phen and **6**-dphphen compounds are similar, with a difference in the incorporation of two phenyl groups on the phen ligand. It follows that the phenyl rings of dphphen ligand play a key role, with torsional freedom, as they are able to twist and become isohelical with the DNA groove [13]. The DNA groove binding is dependent on a combination of hydrogen bonding, van der Waals and electrostatic interactions. In this case, the Hdpa ligand may have a further role in the possible hydrogen bonding of the NH-group with the DNA [13,27].

3.9. Cytotoxicity assay in vitro

The cytotoxicity of the compounds was evaluated against the MDA-MB-231 tumor cell line and V79–4, a non-tumor cell line, using the MTT cell survival assay [44]. The IC_{50} values of the compounds were calculated and are listed in Table 6. Cisplatin was used as a positive control. All complexes showed cytotoxicity, in vitro, against the MDA-MB-231 cell line. The IC_{50} of ruthenium phosphine complexes are much lower than their respective polypyridyl ligands against all tumor cell lines, demonstrating that the structure of the complexes as a whole is very important to define their cytotoxicities [23c.]. The cytotoxicity of the complexes studied here follows two distinct groups: first, the complexes (**1**), (**3**), (**4**), (**5**) and (**6**) with a diimine as co-ligand, which show IC_{50} 1.65–5.66 μM; second; compound **2** containing the aliphatic diamine ligand, which is much less cytotoxic than the other compounds. Thus, the complexes with the diimine ligands are clearly more cytotoxic than the compound possessing aliphatic diamine ligand. This behavior can be explained by the lowest lipophilicity of complex 2, when compared with the others (see lipophilicity data in Table 6).

All the complexes were more cytotoxic against the cancer cell line than the non-tumor cell line. Complex **6** exhibited the highest cytotoxicity against both cells, non-tumor cell and tumor cells, among all six

Table 6
In vitro anticancer activity of complexes **1–6,** and cisplatin, against V79–4 and MDA-MB-231 cell lines, after 48 h incubation period[a].

	Cytotoxicity, IC_{50} (μM)[b]		Lipophilicity	
Compound	MDA-MB-231	V79–4	IS[c]	(LogP)
1	05.66 ± 0.22	> 100	> 18	−0.43 ± 0.03
2	25.50 ± 0.50	> 50	> 2	−0.95 ± 0.08
3	04.25 ± 0.32	27.24 ± 1.63	6	−0.09 ± 0.02
4	02.42 ± 0.09	09.94 ± 2.26	4	−0.06 ± 0.02
5	03.30 ± 0.01	> 50	> 15	−0.04 ± 0.01
6	01.65 ± 0.01	03.08 ± 0.47	2	0.51 ± 0.04
cisplatin	02.44 ± 0.20	21.60 ± 1.28	9	

[a] Data are expressed as mean ± SD (n = 4).
[b] For the free ligands, in all cases, the IC_{50} > 100 μM.
[c] IS = IC_{50}V79–4/IC_{50}MDA-MB-231.

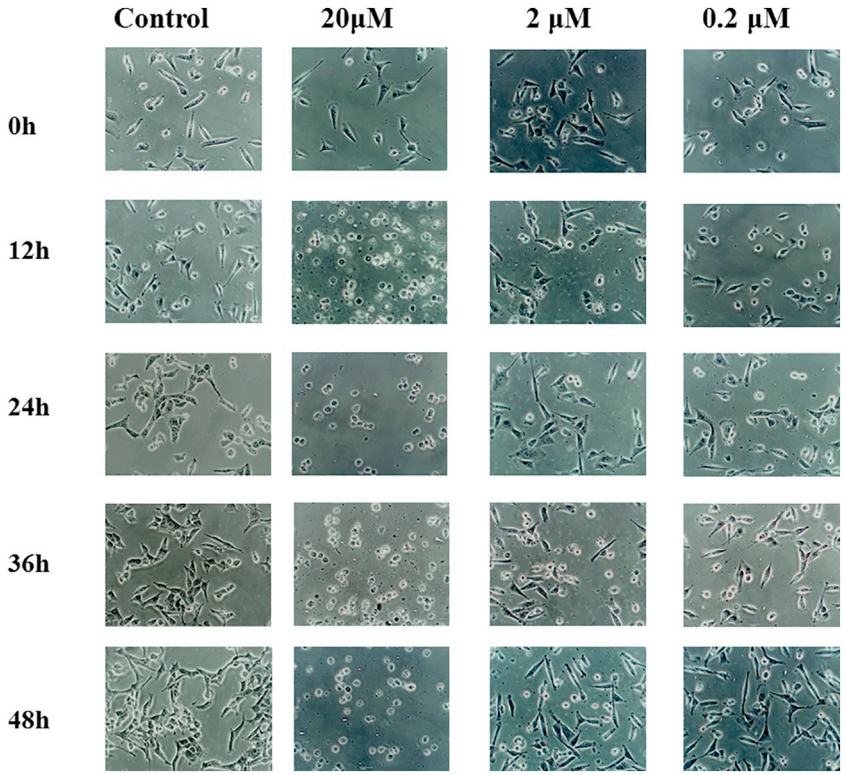

Fig. 7. Cellular morphology of MDA-MB-231. Cells were allowed to grow in a humidified incubator at 37 °C in 5% CO_2 overnight and were then treated with complexes **6** (0.2, 2.0 and 20 μM) for 12, 24, 36 and 48 h. Cell morphology was examined under an inverted microscope at 100× magnification.

complexes. A general relationship can be established between the interaction of the complexes with DNA and their biological activity. Complex 6 is the only one that causes a significant change in the structure of the DNA molecule, and possibly its DNA binding affinity may be an important recognition of its high anticancer activity in both cells.

Most importantly, compounds **1** and **5**, exhibited much higher cytotoxicity in the MDA-MB-231 tumor cell line than in the V97–4 non-tumor cells. The complexes display a marked index selectivity (IS), value of 18 and 15, respectively. These results demonstrated that, in general, compounds **1** and **5** are less toxic than cisplatin in non-tumor cells. Furthermore, analyzing the results of cytotoxicity and the interaction studies of complex-DNA, this suggests that the DNA may not be the only one target for compounds **1–6**. The mode of action of these complexes can involve other biological targets, mainly targets that are overexpressed in tumor cells, explaining the good selectivity of the compounds. Our group has demonstrated that some ruthenium phosphine complexes are able to inhibit the human topoisomerase IB [24], and this enzyme can be considered a potential biological target for complexes **1–6**.

3.10. Lipophilicity

Lipophilicity is the most important property that governs the pharmacokinetics and the pharmacodynamics of drugs. It is directly related to the ability of a compound to permeate through biological membranes. The values of distribution coefficient (Log P) for the complexes 1–6 are shown in Table 6. The complexes 1 and 2 were the ones that presented better affinity for the aqueous phase, being a possible explanation for the higher values of IC_{50} in both cells. While, compounds 3–5 showed nearly equal distribution in both the aqueous and organic phases. However, the complex 6 showed greater lipophilic character and displayed better cytotoxicity activity in both cells as well.

3.11. Morphological study

The analysis of morphological changes is a preliminary study to evaluate cell morphology, adhesion and modifications to the spindle shape of the MDA-MB-231 cells at different concentrations of a complex and during the time. The MDA-MB-231 breast cancer cells in the control group presented a spindle-shaped phenotype and there were few round cells. Compound **6** does not lead to a modification of the MDA-MB 231 cell morphology after 24 h of incubation, compared with control cells (Fig. 7). However, after 48 h of incubation, the morphology was significantly altered in MDA-MB-231 cells, involving a loss of adhesion, modifications to the spindle-shaped form, decreased confluence and reduced cell numbers. There were more round cells, when compared to the control cells, which is indicative of cell detachment, probably due to apoptotic cell death.

4. Conclusions

A new series of ruthenium (II) phosphine complexes of general formula

$[RuCl(PPh_3)(Hdpa)(N{-}N)]Cl$ was synthesized and characterized and it was demonstrated that the nature of the N—N co-ligands is relevant with respect to the cytotoxic activity of the complexes, as well as their binding with the DNA and HSA molecules. Studies on NMR spectroscopy showed that the complexes containing diimine as a co-ligand (**1, 3–6)** are stable in aqueous media by at least 96 h. Compound **2**, containing the aliphatic diamine, the 1,2-diaminoethane, as co-ligand, partially releases the Cl^- ligand, forming the corresponding aqua species. In MTT cytotoxicity studies, complexes **1–6** exhibited good cytotoxicity against the MDA-MB-231 tumor cell line and low activity against the V79–4 non-tumor cell line. Surprisingly, the complexes having a diimine as a co-ligand, which are only slightly or not soluble in water, are more cytotoxic against cancer cells than compound **2,** which has an aliphatic diamine as a co-ligand and is soluble in this solvent.

Furthermore, the facility of compound **2** to suffer hydrolysis in aqueous media, and its ability to form hydrogen bonds, due to the presence of the aliphatic diamine in its structure, did not show better DNA binding affinity and improvement in its cytotoxic activity, when compared to other complexes, which do not suffer hydrolysis.

The results of this study show a correlation between the ability of theses complexes to interact with CT-DNA and HSA and their cytotoxic activity. The relatively high K_b values for the complexes are reflected moderate to strong interactions with the HSA by hydrophobic interactions, suggesting that the absorption and distribution to various tissues can be feasible. The data obtained clearly show that dphphen compound **6** exhibits the highest DNA binding affinity among all the compounds. Besides, complex **6** causes changes in the DNA conformation via binds of the groove of the DNA, which might be explained by the presence of the phenyl rings of dphphen ligand with torsional freedom so that they are able to twist and become isohelical with the DNA groove. Compounds **1–5** exhibited weak electrostatic interactions between the monovalent cations and negatively charged phosphates in DNA, suggesting that their anticancer activity are non-DNA-related mechanisms/factors.

Acknowledgments

The authors gratefully acknowledge the support provided by FAPESP, CNPq. This study was financed in part by the Coordenação de Aperfeiçoamento de Pessoal de Nível Superior - Brasil (CAPES) - Finance Code 001. Juan C. Tenorio would like to thank FAPESP (Process N2013/07581-9) for the PhD grant and financial support.

Conflict of interest

The authors declare no competing financial interest.

Appendix A. Supplementary data

Supplementary data associated with this article can be found in the online version. Crystallographic data of complexes **1**, **2** and **4** can be obtained free of charge from The Cambridge Crystallographic Data Centre: CCDC 1823193 (**1**), 1,823,194 (**2**) and 1,823,196 (**4**). Supplementary data to this article can be found online at doi:https://doi.org/10.1016/j.jinorgbio.2019.01.006.

References

[1] K.D. Mjos, C. Orvig, Chem. Rev. 114 (2014) 4540–4563.
[2] S. Medici, M. Peana, V.M. Nurchi, J.I. Lachowicz, G. Crisponi, M.A. Zoroddu, Coord. Chem. Rev. 284 (2015) 329–350.
[3] R. Trondl, P. Heffeter, C.R. Kowol, M.A. Jakupec, W. Berger, B.K. Keppler, Chem. Sci. 5 (2014) 2925–2932.
[4] A. Bergamo, G. Sava, Dalton Trans. 40 (2011) 7817–7823.
[5] J.A. Ferreira, A. Peixoto, M. Neves, C. Gaiteiro, C.A. Reis, Y.G. Assaraf, L.L. Santos, Drug Resist. Updat. 24 (2016) 34–54.
[6] T. Gianferrara, I. Bratsos, E. Alessio, Dalton Trans. (2009) 7588–7598.
[7] A.C. Komor, J.K. Barton, J. Am. Chem. Soc. 136 (2014) 14160–14172.
[8] A.G. Weidmann, A.C. Komor, J.K. Barton, Comments Inorg. Chem. 34 (2014) 114–123.
[9] S.N. Georgiades, R. Vilar, Ann. Rep. Sect. A, Inorg. Chem. 106 (2010) 481–503.
[10] B.J. Pages, D.L. Ang, E.P. Wright, J.R. Aldrich-Wright, Dalton Trans. 44 (2015) 3505–3526.
[11] M. Sirajuddin, S. Ali, A. Badshah, J. Photochem. Photobiol. B 124 (2013) 1–19.
[12] K. Suntharalingam, R. Vilar, Ann. Rep. Sect. A, Inorg. Chem. 107 (2011) 339–358.
[13] M.R. Gill, J.A. Thomas, Chem. Soc. Rev. 41 (2012) 3179–3192.
[14] P. Venkat Reddy, M.R. Reddy, S. Avudoddi, Y. Praveen Kumar, C. Nagamani, N. Deepika, K. Nagasuryaprasad, S.S. Singh, S. Satyanarayana, Anal. Biochem. 485 (2015) 49–58.
[15] A. Weiss, R.H. Berndsen, M. Dubois, C. Müller, R. Schibli, A.W. Griffioen, P.J. Dyson, P. Nowak-Sliwinska, Chem. Sci. 5 (2014) 4742–4748.
[16] D.R. Boer, L. Wu, P. Lincoln, M. Coll, Angew. Chem. Int. Ed. 53 (2014) 1949–1952.
[17] J.G. Vos, J.M. Kelly, Dalton Trans. (2006) 4869–4883.
[18] T. Biver, C. Cavazza, F. Secco, M. Venturini, J. Inorg. Biochem. 101 (2007) 461–469.
[19] B.M. Zeglis, V.C. Pierre, J.K. Barton, Chem. Commun. (2007) 4565–4579.
[20] G.S. Khan, A. Shah, R. Zia ur, D. Barker, J. Photochem. Photobiol. B 115 (2012) 105–118.
[21] J.K. Barton, A. Danishefsky, J. Goldberg, J. Am. Chem. Soc. 106 (1984) 2172–2176.
[22] L. Colina-Vegas, W. Villarreal, M. Navarro, C.R. de Oliveira, A.E. Graminha, P.I. Maia, V.M. Deflon, A.G. Ferreira, M.R. Cominetti, A.A. Batista, J. Inorg. Biochem. 153 (2015) 150–161.
[23] (a) R.S. Correa, K.M. de Oliveira, F.G. Delolo, A. Alvarez, R. Mocelo, A.M. Plutin, M.R. Cominetti, E.E. Castellano, A.A. Batista, J. Inorg. Biochem. 150 (2015) 63–71;
(b) K.M. Oliveira, L.D. Liany, R.S. Corrêa, V.M. Deflon, M.R. Cominetti, A.A. Batista, J. Inorg. Biochem. 176 (2017) 66–76;
(c) J.E. Takarada, A.P.M. Guedes, R.S. Correa, E. de P. Silveira-Lacerda, S. Castelli, F. Iacovelli, V.M. Deflon, A.A. Batista, A. Desideri, Arch. Biochem. Biophys. 636 (2017) 28–41;
(d) B.N. Cunha, L. Colina-Vegas, A.M. Plutín, R.G. Silveira, J. Honorato, K.M. Oliveira, M.R. Cominetti, A.G. Ferreira, E.E. Castellano, A.A. Batista, J. Inorg. Biochem. 186 (2018) 147–156;
(e) W. Villarreal, L. Colina-Vegas, C. Rodrigues de Oliveira, J.C. Tenorio, J. Ellena, F.C. Gozzo, M.R. Cominetti, A.G. Ferreira, M.A.B. Ferreira, M. Navarro, A.A. Batista, Inorg. Chem. 54 (2015) 11709–11720.
[24] M.S. de Camargo, M.M. da Silva, R.S. Correa, S.D. Vieira, S. Castelli, I. D'Anessa, R. De Grandis, E. Varanda, V.M. Deflon, A. Desideri, A.A. Batista, Metallomics 8 (2016) 179–192.
[25] C. Pereira Fde, B.A. Lima, A.P. de Lima, W.C. Pires, T. Monteiro, L.F. Magalhaes, W. Costa, A.E. Graminha, A.A. Batista, J. Ellena, P. Siveira-Lacerda Ede, J. Inorg. Biochem. 149 (2015) 91–101.
[26] R. Saez, J. Lorenzo, M.J. Prieto, M. Font-Bardia, T. Calvet, N. Omenaca, M. Vilaseca, V. Moreno, J. Inorg. Biochem. 136 (2014) 1–12.
[27] a V. Rajendiran, M. Murali, E. Suresh, M. Palaniandavar, V.S. Periasamy, M.A. Akbarsha, Dalton Trans. (2008) 2157–2170;
b G.N. Kaluderović, T. Krajnović, M. Momcilovic, S. Stosic-Grujicic, S. Mijatović, D. Maksimović-Ivanić, E. Hey-Hawkins, J. Inorg. Biochem. 153 (2015) 315–321;
c A. Zianna, G. Psomas, A. Hatzidimitriou, M. Lalia-Kantouri, J. Inorg. Biochem. 163 (2016) 131–142;
d A. Zianna, G. Psomas, A. Hatzidimitriou, M. Lalia-Kantouri, Polyhedron 124 (2017) 104–116;
e P. Štarha, Z. Dvořák, Z. Trávníček, J. Organomet. Chem. 872 (2018) 114–122.
[28] C. Shobha Devi, D. Anil Kumar, S.S. Singh, N. Gabra, N. Deepika, Y.P. Kumar, S. Satyanarayana, Eur. J. Med. Chem. 64 (2013) 410–421.
[29] C. Shobha Devi, P. Nagababu, S. Natarajan, N. Deepika, P. Venkat Reddy, N. Veerababu, S.S. Singh, S. Satyanarayana, Eur. J. Med. Chem. 72 (2014) 160–169.
[30] A. Rilak, I. Bratsos, E. Zangrando, J. Kljun, I. Turel, Z.D. Bugarcic, E. Alessio, Inorg. Chem. 53 (2014) 6113–6126.
[31] R.W.W. Hooft, COLLECT Data Collection Software, Nonius, Delft, 1998.
[32] L. Farrugia, J. Appl. Crystallogr. 45 (2012) 849–854.
[33] Z. Otwinowski, W. Minor, Methods Enzymol. 276 (1997) 307–326.
[34] G.M. Sheldrick, Acta Crystallogr. Sect. A: Found. Crystallogr. 64 (2008) 112–122.
[35] L.J. Farrugia, J. Appl. Crystallogr. 32 (1999) 837–838.
[36] L.J. Farrugia, J. Appl. Crystallogr. 30 (1997) 565.
[37] A.A. Batista, M.O. Santiago, C.L. Donnici, I.S. Moreira, P.C. Healy, S.J. Berners-Price, S.L. Queiroz, Polyhedron 20 (2001) 2123–2128.
[38] M.P. de Araujo, A.T. de Figueiredo, A.L. Bogado, G. Von Poelhsitz, J. Ellena, E.E. Castellano, C.L. Donnici, J.V. Comasseto, A.A. Batista, Organometallics 24 (2005) 6159–6168.
[39] T.A. Stephenson, G. Wilkinson, J. Inorg. Nucl. Chem. 28 (1966) 945–956.
[40] A.M. Pyle, J.P. Rehmann, R. Meshoyrer, C.V. Kumar, N.J. Turro, J.K. Barton, J. Am. Chem. Soc. 111 (1989) 3051–3058.
[41] (a) R.L. Scruggs, P.D. Ross, Biopolymers 2 (1964) 593–609;
(b) E. Baka, J.E.A. Comer, K. Takács-Novák, J. Pharm. Biomed. Anal. 46 (2008) 335–341.
[42] S. Naveenraj, S. Anandan, J Photochem Photobiol C: Photochem Rev 14 (2013) 53–71.
[43] P.D. Ross, S. Subramanian, Biochemistry 20 (1981) 3096–3102.
[44] T. Mosmann, J. Immunol. Methods 65 (1983) 55–63.
[45] W.J. Geary, Coord. Chem. Rev. 7 (1971) 81–122.
[46] G.G. Gastone, P. Gilli, The Nature of the Hydrogen Bond, 1° ed., Oxford University Press, Oxford, 2009.
[47] (a) D.E. Morris, Y. Ohsawa, D.P. Segers, M.K. DeArmond, K.W. Hanck, Inorg. Chem. 23 (1984) 3010–3017;
(b) R.C. Weast, R.C. Handbook of Chemistry and Physics, 67th ed, CRC Press, Inc., Boca Raton, FL, 1986;
(c) H.K. Hall Jr., J. Am. Chem. Soc. 79 (1957) 5441–5444;
(d) D.D. Perrin, Aust. J. Chem. 17 (1964) 484–489.
[48] D.P. Segers, M.K. DeArmond, J. Phys. Chem. B 86 (1982) 3768–3776.
[49] D. Sleep, J. Cameron, L.R. Evans, Biochim. Biophys. Acta 1830 (2013) 5526–5534.
[50] M.K. Helms, C.E. Petersen, N.V. Bhagavan, D.M. Jameson, FEBS Lett. 408 (1997) 67–70.
[51] J.R. Lakowicz, Principles of Fluorescence Spectroscopy, 3° ed., Springer-Verlag US, New York, 2006.
[52] M.B. Moreira, D.S. Franciscato, K.C.F. Toledo, J.R.B.d. Souza, H.S. Nakatani, V.R.d. Souza, Quím. Nova 38 (2015) 227–232.
[53] M.I. Chaudhari, S.B. Rempe, D. Asthagiri, L. Tan, L.R. Pratt, J. Phys. Chem. B 120 (2016) 1864–1870.
[54] G. Hummer, S. Garde, A.E. García, M.E. Paulaitis, L.R. Pratt, J. Phys. Chem. B 102 (1998) 10469–10482.
[55] L.R. Pratt, A. Pohorille, Chem. Rev. 102 (2002) 2671–2692.
[56] M. Nišavić, M. Stoiljković, I. Crnolatac, M. Milošević, A. Rilak, R. Masnikosa, Arab.

J. Chem. (2016), https://doi.org/10.1016/j.arabjc.2016.07.021.
[57] B.S.P. Reddy, S.M. Sondhi, J.W. Lown, Pharmacol. Ther. 84 (1999) 1–111.
[58] S.U. Rehman, T. Sarwar, M.A. Husain, H.M. Ishqi, M. Tabish, Arch. Biochem. Biophys. 576 (2015) 49–60.
[59] Y. Zhang, P.-C. Hu, P. Cai, F. Yang, G.-Z. Cheng, RSC Adv. 5 (2015) 11591–11598.
[60] F. Zsila, Int. J. Biol. Macromol. 72 (2015) 1034–1040.
[61] T.D. McGregor, W. Bousfield, Y. Qu, N. Farrell, J. Inorg. Biochem. 91 (2002) 212–219.
[62] M. Frik, J. Fernandez-Gallardo, O. Gonzalo, V. Mangas-Sanjuan, M. Gonzalez-Alvarez, A. Serrano del Valle, C. Hu, I. Gonzalez-Alvarez, M. Bermejo, I. Marzo, M. Contel, J. Med. Chem. 58 (2015) 5825–5841.
[63] J.M. Kelly, A.B. Tossi, D.J. McConnell, C. OhUigin, Nucleic Acids Res. 13 (1985) 6017–6034.
[64] G.J. Ryan, F.E. Poynton, R.B.P. Elmes, M. Erby, D.C. Williams, S.J. Quinn, T. Gunnlaugsson, Dalton Trans. 44 (2015) 16332–16344.